Liu, Y., Magnall, J. M., Gleeson, S. A., Bowyer, F., Poulton, S. W., Zhang, J. (2020): Spatio-temporal evolution of ocean redox and nitrogen cycling in the early Cambrian Yangtze ocean. - Chemical Geology, 554, 119803.

https://doi.org/10.1016/j.chemgeo.2020.119803

Spatio-temporal evolution of ocean redox and nitrogen cycling in the early Cambrian Yangtze ocean

Yang Liu[a, b*], Joseph M. Magnall[b], Sarah A. Gleeson[b, c], Frederick Bowyer[d], Simon W. Poulton[d], Jinchuan Zhang[a]

[a] School of Energy resource, China University of Geosciences (Beijing), Beijing 100083, China.

[b] GFZ German Research Centre for Geosciences, 14473 Potsdam, Germany.

[c] Institute of Geological Sciences, Freie Universität, 74-100 Malteserstrasse, Berlin 12249, Germany.

[d] School of Earth and Environment, University of Leeds, Leeds LS2 9JT, UK.

Corresponding Author: yangliu@cugb.edu.cn

Abstract

The early Cambrian was a critical interval for the Earth system, during which a rise in oceanic and atmospheric oxygen levels coincided with the rapid diversification of metazoans. A variety of contrasting models have been proposed for the spatiotemporal redox evolution of the early Cambrian ocean. These include the development of a well-oxygenated deep ocean at the base of Cambrian Stage 3 (commencing at ~521 Ma), or alternatively, persistent and widespread anoxic (ferruginous) conditions throughout the early Cambrian ocean. Here, we present redox sensitive trace element (RSTE), Fe speciation, and N and C isotope ($\delta^{15}N_{sed}$ and $\delta^{13}C_{org}$) data for samples from a section (Zhongnancun) of the early Cambrian Niutitang Formation, which was deposited on the outer-shelf of the Yangtze Block, South China. The Fe speciation and RSTE data provide evidence of a transition from euxinic, through ferruginous, to oxic conditions during deposition of the Niutitang Formation. The combination of these new data with existing data from the inner-shelf to basin environment, implies regional redox stratification across the Yangtze Block during Cambrian stages 2 and 3, with oxic shallow waters above ferruginous deep waters, and spatial variability in the degree of mid-depth euxinia. Oxygenation of deeper waters may have occurred by early Cambrian Stage 4 (~514 Ma). A compilation of $\delta^{15}N$ values from multiple early Cambrian sections of the Yangtze Block indicate that N_2 fixation dominated the nitrogen cycle during late Cambrian Stage 2. Low $\delta^{15}N$ values (< -2‰) preserved in shelf sections can be interpreted to represent partial assimilation of NH_4^+, where NH_4^+ was not a limiting nutrient. During the early-middle Cambrian Stage 3, more positive $\delta^{15}N$ values (0 to +3‰) are recorded in shelf sections, with lower values (-2 to +2‰) recorded in slope-basin sections. The positive $\delta^{15}N$ values observed in shelf sections are likely a consequence of partial denitrification in the water column, whereas coeval deeper water $\delta^{15}N$ values of ~0‰ may reflect the dominance of N_2 fixation. The distribution of $\delta^{15}N$ values, combined with a gradient in $\delta^{13}C_{org}$ values, are consistent with a

stratified ocean model. The $\delta^{15}N$ values of all sections are lower than those of the modern ocean, which may indicate that the nitrate concentration of the early Cambrian Yangtze ocean was generally low during Cambrian Stage 3. The observed gradient in $\delta^{15}N$ values is similar to that observed in records from Mesoproterozoic oceans, suggesting that abundant nitrate availability may have been restricted to shelf environments. We propose that increased nitrogen availability in shelf settings may have contributed to the evolution of large-celled eukaryotic phytoplankton. This provided a positive feedback on ocean oxygenation, allowing for increased complexity in early animal ecosystems on the continental shelf, and ultimately deep water oxygenation.

Key words: Nitrogen isotopes; Redox conditions; Nitrogen cycle; Early Cambrian; South China.

1. Introduction

The early Cambrian (~529 - 514 Ma, late Fortunian to early Stage 4) encompasses an interval of major evolutionary innovation, including the rapid diversification of crown group Metazoa, against a backdrop of global climatic instability and variability in the chemical composition of the oceans and atmosphere (Krause et al., 2018; He et al., 2019; Wood et al., 2019). Perhaps most significantly, Cambrian Stage 3 in South China includes the radiation of crown group bilateria and non-bilateria, alongside preservation of the

Chengjiang Lagerstatte (Wood et al., 2019). This interval also immediately precedes the global Sinsk extinction event (Zhuravlev and Wood, 1996; He et al., 2019).

The number of studies attempting to more precisely constrain the spatial and temporal redox evolution of the early Cambrian ocean has increased in recent years. Multiple studies have focused on platform to basin reconstructions of the Yangtze Block (South China) with integrated sequence stratigraphy, resulting in broad spatial constraints on the redox evolution of these depositional environments. During the early Cambrian there is widespread evidence for anoxic ferruginous conditions, as constrained by a number of different proxies, including Fe speciation (Goldberg et al., 2007; Canfield et al., 2008; Och et al., 2016; Li et al. 2017; Hammarlund et al., 2017), redox-sensitive trace elements (Xu et al., 2012; Jin et al., 2016), and sulfur isotope compositions (Feng et al., 2014). A stepwise expansion of oxic water column conditions from shallow to deep settings is then recorded across the Yangtze Block through Cambrian Stages 2 to 4, albeit with continued evidence for locally ferruginous conditions in deeper water settings (Li et al. 2017; Hammarlund et al., 2017). The preservation of near-modern seawater $\delta^{98/95}Mo$ values (~2.34‰) recorded in black shales, however, has been used as evidence of an expanded oxic sink for Mo in the global oceans by Cambrian Stage 3 (~521 Ma, Chen et al., 2015; Wen et al., 2015). Wang et al. (2018) suggested that oxygenation of the deep ocean occurred during Cambrian

Stage 3, based on a comprehensive N isotope dataset from the Yangtze Block.

One of the main challenges associated with interpreting geochemical redox proxies relates to discriminating between local and global conditions, and combining both temporal and spatial variability. Recently, geochemical and paleontological data from multiple stratigraphic sections were integrated in a sequence stratigraphic framework to reconstruct spatio-temporal redox evolution along a Cambrian basin margin sequence from the Baltic Sea (Guilbaud et al. 2018). In their study, Guilbaud et al. (2018) argued for the development of an oxygen minimum zone (OMZ) along a productive continental margin. A euxinic wedge could be dynamically maintained above deeper ferruginous waters, if sufficient sulfate and organic matter were available (Poulton et al., 2010; Poulton and Canfield, 2011; Li et al., 2018). The OMZ model has also been applied to stratigraphic sequences from the Yangtze Block (e.g. Hammarlund et al. 2017). However, there has been limited evaluation as to the spatial extent of this redox architecture across the Yangtze Block, or higher order stratification with respect to intermediate redox states (in addition to oxic, anoxic and euxinic conditions). For example, aerobic conditions in the surface ocean may have overlain deeper nitrogenous waters, with manganous (Tostevin et al., 2016) and then ferruginous water column conditions below, as electron acceptors were utilized in order of their energy yield during organic carbon remineralization.

Iron speciation (Poulton and Canfield, 2005) is a particularly robust proxy used for reconstructing local depositional redox conditions (e.g., Poulton et al., 2004; Canfield et al., 2007; Poulton and Canfield, 2011). When combined with redox-sensitive trace element (RSTE) concentrations and ratios (Tribovillard et al., 2006; Algeo and Rowe, 2012), a detailed characterisation of the precise nature of ocean redox chemistry can be achieved. In addition, nitrogen isotopes ($\delta^{15}N$) are sensitive to productivity in the photic zone, and the isotopic signature of biomass produced in the photic zone may ultimately be preserved in sediments. The redox structure of the ocean exerts a strong control on the speciation of dissolved inorganic nitrogen, with NO_3^- being stable in oxic waters and NH_4^+ being stable in anoxic waters (Ader et al., 2016). As such, $\delta^{15}N$ values are increasingly being utilized in studies of seawater paleoredox in both the Phanerozoic and Precambrian (e.g. Algeo et al., 2008; Godfrey and Falkowski, 2009; Higgins et al., 2012; Godfrey et al., 2013; Stüeken, 2013; Ader et al., 2016; Stüeken et al., 2016; Zerkle et al., 2017).

In this study, we report Fe speciation, RSTE, $\delta^{15}N_{sed}$ and $\delta^{13}C_{org}$ values from a new outer-shelf outcrop section of Cambrian stratigraphy from the Yangtze Block. We compile our new data with previously published data from correlative sections, to present a more comprehensive model for the spatial and temporal evolution of nitrogen cycling in the early Cambrian Yangtze ocean. Subsequently, we evaluate possible links between nitrogen availability, marine paleoredox and biological evolution during this key interval of Earth history.

2. Geological setting

Neoproterozoic and early Cambrian marine sedimentary rocks are well preserved in the Yangtze Block, South China. According to palaeomagnetic records, South China was at low-latitudes during the early Cambrian (Merdith et al., 2017). Paleogeographic reconstructions show that the environmental setting of the Yangtze Block comprised platform facies, a transition zone, and slope to basin facies, as illustrated in Fig. 1 (Steiner et al., 2001; Jiang et al., 2012). The lower Cambrian Niutitang Formation and equivalent strata unconformably overly the upper Ediacaran Dengying Formation. The Niutitang Formation is dominantly comprised of black shale, but the lower parts of the Formation contain bedded phosphorite, barite, and thick units (up to tens of meters) of "stone coal" (combustible shale of algal origin, Xu et al., 2012). Furthermore, in Guizhou and Hunan Province, an organic-rich, Ni-Mo sulfide layer with a maximum thickness of 30 cm is used as a marker horizon for the lowermost part of the Niutitang Formation (Jiang et al., 2006; Xu et al., 2012). Previous studies have evaluated the thermal maturity of organic matter to show the Niutitang Formation has only undergone sub-greenschist (prehnite-pumpellyite) facies metamorphism (Kříbek et al., 2007).

The Zhongnancun section in this study is located in Zunyi city, Guizhou province (N 27°41′21.4″, E 106°40′67.0″), and paleo-geographically lies in the transition zone (outer-shelf) (Fig. 1, Pi et al., 2013). The Niutitang Formation at this section has been divided into 3 intervals according to lithostratigraphic analysis. Interval 1 contains a variety of rock types, including brownish to black, siliceous phosphorite (~65 cm in thickness), a K-bentonite layer interbedded with black chert (~20 cm in thickness), carbonaceous chert interbedded with black shale (~1.70 m in thickness), and carbonaceous shale (~2.90 m in thickness). The K-bentonite layer at the Zhongnancun section has been dated using the SHRIMP U-Pb method to 532.3 ± 0.7 Ma (Jiang et al., 2009). The phosphorite deposits and nodules hosted by Lower Cambrian shale across the Yangtze Block may have resulted from the interaction of upwelling P-replete water with oxygenated surface waters (Wille et al., 2008). The origin of the widespread Ediacaran-Cambrian (E-C) chert deposits in the Yangtze block has recently been revealed by silicon isotopes, indicating that seawater was the primary silica source of the cherts (Gao et al., 2020).

The base of Interval 2 is marked by the aforementioned Ni-Mo sulfide layer (~15 cm thick), which is considered to belong to Cambrian Stage 2 based on biostratigraphic data (Steiner et al., 2001). A Re-Os isochron age of 521 ± 5 Ma has been reported for the sulfide ore from three mining sites (Sancha in Hunan province, and Dazhuliushui and Maluhe in Guizhou province) (Xu et al., 2011), confirming the biostratigraphic age. The Ni-Mo sulfide layer is considered to have been deposited under euxinic conditions (Lehmann et al., 2007; Steiner et al., 2001) but the origin of the metal enrichment is debated. Previous studies have suggested that the sulfide layer may be a product of hydrothermal venting (Steiner et al., 2001; Jiang et al., 2006) versus scavenging from seawater by organic matter (Lehmann et al., 2007; Xu et al., 2011). The potential effects of volcanic input on early Cambrian black shale and sulfide ore of South China has been indicated by mercury isotopes, suggesting that Hg in these rocks mainly originated from seawater (Yin et al., 2017). The remainder of Interval 2 consists of ~16 m of black shale, overlain by Interval 3, which is dominated by dark gray to black silty shale with a thickness of ~12 m.

3. Materials and methods

A total of 39 samples (~1 kg each) were collected from the lower Cambrian Niutitang Formation at the Zhongnancun outcrop section, including three chert samples, one sulfide ore sample and 35 shale samples. These samples were carefully trimmed to remove possible weathered surfaces. Approximately 300 – 500 g of remaining material from each sample was then crushed to a fine powder (<74 μm) using an agate mortar.

Total organic carbon (TOC) concentrations were determined on a LECO CS-230 carbon and sulfur analyzer at the Geochemistry Laboratory of Yangtze University. Prior to analysis, samples were subjected to a pre-leach in 6 M HCl for 24 hrs, in order to remove carbonate. Major and trace elements were analyzed using XRF (AB104L, AL104, AxiosmAX) and ICP-MS (PerkinElmer, Elan DCR-e), respectively, at the Beijing Research Institute of Uranium

Geology. Detailed descriptions of the methods have been published by Gao et al. (2015). For ICP-MS analysis, approximately 50 mg of powdered samples were treated with a solution mixture of 2 ml HNO_3, 3 ml HF and 1 ml HCl at 150°C. After drying, the residues were treated with 1 ml HNO_3 and 3 ml HF at 180°C for 48 h. After samples were dissolved, each solution was cooled and 0.5 ml $HClO_4$ (70%) was used to oxidize organic matter. After evaporation, residues were re-dissolved in 2 ml HNO_3 for analysis. Analytical errors are generally better than 10% for Fe_T and Al, and ±5% for trace elements. Trace metal enrichment factors (Mo_{EF} and U_{EF}) were calculated using the formula: $X_{EF} = (X/Al)_{sample}/(X/Al)_{AUCC}$, where X = Mo or U, and AUCC refers to the composition of average upper continental crust (McLennan, 2001).

Iron speciation was conducted to reconstruct water column palaeoredox conditions. Highly reactive iron (Fe_{HR}) was determined as the sum of four operationally-defined pools, predominantly comprising pyrite Fe (Fe_{py}), carbonate-associated Fe (Fe_{carb}), ferric oxide Fe (Fe_{ox}), and magnetite Fe (Fe_{mag}) (Poulton et al., 2004; Poulton and Canfield, 2011). Fe_{carb}, Fe_{ox} and Fe_{mag} were determined via the sequential extraction procedure of Poulton and Canfield (2005). Approximately 100 mg of sample powder was first subjected to a sodium acetate leach (buffered to pH = 4.5 with acetic acid) at 50 ºC for 48 hours for the extraction of Fe_{carb}. The sample residue was then leached in sodium dithionite (50 g/L sodium dithionite, 58.82 g/l sodium citrate and 20 ml/l acetic acid) at room temperature for 2 hours, to extract Fe_{ox}. Finally, the remaining solid sample was treated with ammonium oxalate solution (0.2 M ammonium oxalate and 0.17 M oxalic acid) at room temperature for 6 hours, to extract Fe_{mag}. All extraction solutions were measured at the Beijing Research Institute of Uranium Geology by atomic absorption spectroscopy (AAS), with RSDs of <5% for Fe in all fractions. Fe_{py} was calculated from the pyrite sulfur extracted as an Ag_2S precipitate following the chromium reduction method (Canfield et al., 1986).

Organic carbon and nitrogen isotope ratios were measured using a Thermo Finnigan MAT 253 isotope ratio mass spectrometer interfaced to a Flash EA 2000 elemental analyzer and a Conflo IV continuous flow interface at the Beijing Research Institute of Uranium Geology. For organic carbon isotope measurements, 50 – 100 mg of sample was weighed and digested in 2 mol/L HCl to ensure complete carbonate removal. Residues were washed with distilled water to remove chlorides and dried at 70°C for 8 h. The decalcified sample powder was then weighed into tin capsules for organic carbon isotope measurements. Carbon isotope values ($\delta^{13}C_{org}$) are reported in per mil relative to the international VPDB (Vienna Pee Dee Belemnite) standard. The analytical uncertainties were monitored by two international standards (USGS40, $\delta^{13}C$ = −26.39‰; IAEA-600, $\delta^{13}C$ = −24.8‰) and a China national standard (GSW04407, $\delta^{13}C$ = −22.43‰), with replicate analyses yielding a standard deviation of ±0.3‰ for $\delta^{13}C_{org.}$

Samples for N isotope analysis were first analyzed for their total nitrogen content (TN). Only those samples with TN >0.012 mg (>0.006%) were considered to provide reliable nitrogen isotope results (Wang et al., 2015). Approximately 30 – 150 mg of each bulk sample powder was weighed into a tin capsule and a carbon-absorbing trap was used in the EA to avoid interferences during the analysis due to the low N content and high C content of the marine shale samples. The nitrogen isotopic composition of sedimentary rocks ($\delta^{15}N_{sed}$) is reported in per mil relative to atmospheric N_2. The analytical uncertainties were monitored by three international standards (USGS40, $\delta^{15}N$ = −4.52‰; IAEA-600, $\delta^{15}N$ = +1.0‰; IAEA-N-2, $\delta^{15}N$ = +20.3‰) with replicate analyses yielding a standard deviation of ±0.4‰ for $\delta^{15}N$.

4. Results

Nitrogen ($\delta^{15}N_{sed}$) and organic carbon ($\delta^{13}C_{org}$) isotopes, total organic carbon (TOC), total nitrogen (TN), Fe speciation, and redox-sensitive trace element (e.g. Mo, U, V) concentrations from the outer-shelf Zhongnancun section are presented in Table S1, and selected stratigraphic trends are illustrated in Fig. 2.

Three chert samples, eight black shale samples and one sulfide ore sample were analysed from Interval 1. The three chert samples contain relatively low TOC, TN and RSTE concentrations, ranging from 0.82 to 1.21 wt.% (mean = 1.03 wt.%) for TOC, from 0.05 to 0.09 wt.% (mean = 0.07 wt.%) for TN, from 4.1 to 4.8 ppm (mean = 4.5 ppm) for U, from 101 to 480 ppm (mean = 297 ppm) for V, and from 6.8 to 18.5 ppm (mean = 12.2 ppm) for Mo. The Fe_T concentrations for chert samples range from 0.68 to 0.76 wt.%, the Fe_{HR}/Fe_T and Fe_{Py}/Fe_{HR} values range from 0.28 to 0.41 and 0.04 to 0.05, respectively.

The black shales from Interval 1 are characterized by higher TOC, TN and RSTE concentrations. The TOC values range from 4.27 to 12.08 wt. (mean = 7.69 wt.%), TN values range from 0.09 to 0.16 wt.% (mean = 0.12 wt.%), U concentrations range from 23.8 to 112 ppm (mean = 40.0 ppm), V concentrations range from 1211 to 4872 ppm (mean = 2594 ppm), and Mo concentrations range from 74.3 to 208 ppm (mean = 119 ppm). The Mo/TOC ratios are between 8 and 21 (mean = 17). The sulfide ore sample preserves high TOC (10.72 wt.%), TN (0.12 wt.%) and RSTE concentrations (41850 ppm for Mo, 612 ppm for V, and 120 ppm for U), with a high Mo/TOC ratio (3904). The Fe_T concentrations for shale samples range from 1.76 to 11.50 wt.%, and Fe_{HR}/Fe_T and Fe_{Py}/Fe_{HR} values for black shales range from 0.67 to 0.89 and 0.66 to 0.85, respectively. The $\delta^{13}C_{org}$ values in Interval 1 preserve a prominent negative excursion from -31.2‰ down to a nadir of -33.8‰. Values for $\delta^{15}N_{sed}$ are between +1.2 to -0.6‰, with the exception of a prominent outlier at -4.2‰.

In comparison to Interval 1, black shale samples of Interval 2 generally preserve lower TOC (with the exception of two samples at the bottom of this interval), TN and RSTE concentrations. Total organic carbon concentrations are in the range 3.14 to 15.56 wt.% (mean = 5.39 wt.%), and TN ranges from

0.06 to 0.13 wt.% (mean = 0.09 wt.%). The concentration of U is in the range 19.2 to 68.6 ppm (average = 29.9 ppm), V ranges from 362 ppm to 1453 ppm (mean = 972 ppm), Mo ranges from 7.3 ppm to 125 ppm (mean = 41.1 ppm), and Mo/TOC is in the range 2 to 15 ppm/wt% (mean = 7 ppm/wt%). The Fe_T concentrations range from 0.78 to 2.32 wt.%, and Fe_{HR}/Fe_T and Fe_{Py}/Fe_{HR} ratios range from 0.38 to 0.88 and 0.01 to 0.72, respectively. Values for $\delta^{13}C_{org}$ initially increase following the negative excursion exhibited in Interval 1, from -32.1 to -29.6‰, before decreasing once more to -31.4‰ near the top of Interval 2. Values for $\delta^{15}N_{sed}$ vary between +0.6 and +2.7‰, and exhibit an overall positive excursion in this interval.

Silty black shales of Interval 3 preserve the lowest TOC, TN and RSTE concentrations of the three intervals. The TOC concentrations range from 1.32 to 2.73 wt.% (mean = 1.98 wt.%), and TN values range from 0.06 to 0.11 wt.% (mean = 0.09 wt.%). The concentration of U is in the range 15.2 to 27.3 ppm (mean = 19.0 ppm), V ranges from 252 to 856 ppm (mean = 446 ppm), Mo ranges from 4.5 to 14.8 ppm (mean = 8.6 ppm), and the Mo/TOC ratio is in the range 3 – 6 ppm/wt% (mean = 4 ppm/wt%). The Fe_T concentrations range from 1.25 to 2.46 wt.%, and Fe_{HR}/Fe_T and Fe_{Py}/Fe_{HR} values range from 0.21 to 0.48 and 0.11 to 0.42, respectively. Values for $\delta^{13}C_{org}$ in Interval 3 are relatively invariant, and range from -30.5 to -30.0‰, whilst $\delta^{15}N_{sed}$ decreases from +1.1 to +0.2‰.

5. Discussion

5.1. Palaeoredox evolution of the early Cambrian Nanhua Basin

The ratio Fe_{HR}/Fe_T, together with the extent of sulfidation of the highly reactive iron pool (Fe_{Py}/Fe_{HR}), can provide valuable information about local bottom water redox conditions (e.g. Poulton et al., 2004; Canfield et al., 2008; Poulton and Canfield, 2011). Generally, Fe_{HR}/Fe_T ratios > 0.38 suggest anoxic water column conditions, with ratios < 0.22 providing strong support for oxic depositional conditions (Raiswell and Canfield, 1998; Raiswell et al., 2001; Poulton and Raiswell, 2002: Poulton and Canfield, 2011). Enrichments in Fe_{HR} (i.e. Fe_{HR}/Fe_T > 0.38) commonly occur under anoxic conditions due to water column precipitation of either Fe sulfide minerals (in euxinic settings) or non-sulfidized Fe minerals (in anoxic ferruginous settings) (Canfield et al., 1996; Raiswell and Canfield, 1998; Poulton et al., 2004; Poulton and Canfield, 2011). Fe_{HR}/Fe_T ratios between 0.22 – 0.38 are considered equivocal due to the potential dilution of Fe_{HR} enrichments either as a consequence of rapid sedimentation or post-depositional transfer of unsulphidized Fe_{HR} to Fe-rich clay minerals during early diagenesis (e.g. Poulton and Raiswell, 2002; Poulton et al., 2010). In such cases, additional insight into depositional redox conditions may be gained from Fe/Al ratios and RSTE systematics (e.g. Doyle et al., 2018). For sediments deposited under anoxic water column conditions, Fe_{Py}/Fe_{HR} ratios of < 0.7 and > 0.7-0.8 are commonly used to distinguish between ferruginous and euxinic conditions, respectively (e.g.

Poulton et al., 2004; Poulton and Canfield, 2011; Raiswell and Canfield, 2012). It is necessary to carefully consider the lithology when applying Fe based redox proxies (Raiswell et al. 2018). For lithologies where clastic input has been diluted (e.g. carbonates, cherts) threshold values for total iron and organic carbon (> 0.5% for both) have been proposed as minimum requirements for using the iron-based redox proxies (e.g. Clarkson et al., 2014; Raiswell et al. 2018). The Fe_T and TOC concentrations in all samples from this study are greater than 0.5%, indicating that the iron speciation proxy is a valid approach for reconstructing depositional paleoredox conditions.

At the Zhongnancun section, black shale samples from Interval 1 have elevated Fe_{HR}/Fe_T (0.67-0.89), with generally high Fe_{Py}/Fe_{HR} (0.66-0.85), which is consistent with anoxic water column conditions, and at least intermittent euxinia. Elevated Fe_{HR}/Fe_T and a decrease in Fe_{Py}/Fe_{HR} supports a shift to dominantly ferruginous conditions up-section into Interval 2 (Fig. 2). Samples from Interval 3 have Fe_{HR}/Fe_T ratios that fall in the equivocal zone (except for one sample at 33.4 m, where $Fe_{HR}/Fe_T = 0.48$), and we thus utilize RSTE systematics to provide additional insight into water column redox conditions during deposition of these samples.

The degree to which Mo, U and V are enriched in organic-rich mudstones (ORMs), alongside co-variation in total organic carbon (TOC), can be effectively used to track both depositional paleoredox conditions and the size of seawater trace metal reservoirs (Algeo and Lyons, 2006; Anbar et al., 2007;

Scott et al., 2008; Sahoo et al., 2012). Starting with samples from Interval 1 (Fig. 2), the high level of Mo enrichment (mean for black shale samples = 119 ppm) is consistent with the presented Fe speciation data, and suggests dominantly euxinic conditions (e.g. Scott and Lyons, 2012). However, the co-variation between Mo and TOC is not particularly strong (R^2 = 0.41; Fig. 3a), which might be consistent with variable water column H_2S concentrations, since persistently high H_2S is required to effectively draw down Mo (Tribovillard et al., 2006). Indeed, variability in H_2S concentrations would be consistent with our Fe speciation data, whereby some of the Fe_{Py}/Fe_{HR} ratios fall slightly below the 0.7 threshold for robust identification of water column euxinia, implying more limited sulfide availability. As with Mo, however, enrichments in V (612 to 4872 ppm, average 2373 ppm) for ORMs from Interval 1 (Fig. 2) are consistent with generally euxinic water column conditions (Tribovillard et al., 2006).

The Mo and TOC enrichments in Interval 2 remain high, but are lower than those of Interval 1 (Fig. 2), consistent with the interpretation of anoxic ferruginous conditions from Fe speciation data. Uranium is not commonly enriched under oxic/dysoxic conditions, but is instead present primarily as carbonate complexes that are chemically unreactive (see references in Algeo and Tribovillard, 2009). Strong U enrichment does, however, occur under anoxic conditions, where enrichments commonly show a positive correlation with TOC (Fig. 3b; Algeo and Tribovillard, 2009). By contrast, the positive correlation (R^2 = 0.66) between Mo and TOC, together with relatively low Mo concentrations (9 ± 5 ppm; Fig. 3a), provides evidence that Mo was sequestered in association with organic matter in an oxic or dysoxic environment during deposition of Interval 3 (Scott et al., 2008), which suggests that the Fe_{HR}/Fe_T ratios of <0.38 (Fig. 2) are indeed recording oxic/dysoxic water column conditions.

Co-variation between Mo and U in marine basins can provide an additional level of interpretation concerning trace element enrichment mechanisms and possible water mass restriction (e.g. Tribovillard et al., 2006; Algeo and Tribovillard, 2009). Molybdenum and U enrichment factors from the Zhongnancun section are largely consistent with the pattern observed in the modern open ocean (Fig. 4). Samples from Interval 1 exhibit high Mo_{EF}, U_{EF} and Mo/U ratios, which support sedimentary enrichment of Mo and U from a dominantly euxinic water column. Samples from Interval 2 preserve lower concentrations of Mo and U, and some samples have elevated Mo/U ratios relative to the modern open ocean trend, which may suggest a weak particulate shuttle (Algeo and Tribovillard, 2009). The preferential complexation of Mo with Fe-Mn oxyhydroxides can lead to the enhanced transfer of Mo into sediments, thereby resulting in elevated Mo/U ratios (Algeo and Tribovillard, 2009). This particulate shuttle effect is most pronounced where the oxic – anoxic chemocline is located close to the sediment water interface (e.g. modern Baltic Sea, Scholz et al., 2013).

The relative importance of the particulate shuttle for Mo enrichment can be assessed from Mo_{EF} and U_{EF} data compiled for multiple lower Cambrian sections (Fig. 4). The lowest Mo_{EF}, U_{EF} and Mo/U ratios are found in samples from Interval 3, supporting oxic/suboxic conditions. However, it is worth noting that the Mo enrichment associated with the Fe-Mn oxyhydroxide particulate shuttle may also complicate the interpretation of Mo and TOC co-variation (Magnall et al. 2018), and may be an alternative explanation for the lack of correlation between Mo and TOC in Intervals 1 and 2.

The redox constraints from the Zhongnancun section can be compared to other studies conducted on correlative sections (e.g. Jin et al., 2016) from the Yangtze Block (Fig. 5; Table S2). Euxinic conditions prevailed in the transitional zone between oxic waters on the platform and dominantly ferruginous deeper waters on the slope/basin during Cambrian Stage 2. Subsequently, euxinic conditions were progressively replaced by anoxic, non-sulfidic water column conditions as the sea level regression proceeded (early-middle Cambrian Stage 3). Oxic conditions were progressively established in shelf settings during late Cambrian Stage 3 with anoxia largely maintained in slope and basin environments and euxinic conditions in deeper water environments.

These observations are consistent with a stratified ocean model in which euxinic mid-depth waters were dynamically maintained between oxic surface waters and ferruginous deeper waters. Progressive ventilation, first of shallow, and then shelf and slope environments, proceeded during Cambrian Stage 2 to 3 (e.g. Jin et al., 2016; Li et al., 2017). By early Cambrian Stage 4 (~514 Ma), oxic conditions may have been established in shallow shelf (i.e. Jinsha section) and slope settings, and in deeper waters (i.e. Longbizui section), while mid-depth environments (i.e. Wengan and Songtao sections) remained anoxic (Fig. 5), suggesting a redox structure similar to an oxygen minimum zone (OMZ). In terms of the broader redox landscape, geochemical proxies that are sensitive to long term terrestrial weathering processes provide evidence that global tectonic activity during the Ediacaran-Cambrian could have resulted in the increased supply of nutrients to the oceans, primary productivity and associated photosynthetic O_2 release (Campbell and Squire, 2010). Yet it remains an ongoing challenge to differentiate between local, regional, and global scale controls on the spatio-temporal redox evolution of ancient marine systems. In the case of the Yangtze Ocean, for example, a marine regression during Cambrian Stage 3 could have simply resulted in the offshore migration of euxinic waters (e.g. Bowyer et al. 2017). In the following, we evaluate N isotope data from the Zhongnancun section together with compiled data from the literature to further evaluate the redox architecture of the Cambrian Yangtze Ocean.

5.2. Nitrogen cycling in the early Cambrian Yangtze ocean

The isotopic composition of nitrogen ($\delta^{15}N$ values) can provide additional information for studies on seawater paleoredox (Fig. 6). In the modern oceans, the primary source of bioavailable nitrogen to the marine system is via fixation of atmospheric N_2 (N_2-fixation), which transforms molecular N_2 into organic matter (via NH_4^+) through ammonification. There is negligible isotopic fractionation associated with ammonification (-1‰ on average), however under Fe^{2+}-rich or thermophilic conditions, fractionation may be as large as -4‰ (e.g. Zerkle et al., 2008; Zhang et al., 2014). In oxic environments, the NH_4^+ released by breakdown of organic matter is rapidly oxidized to NO_2^- and then to NO_3^- through nitrification, also with negligible fractionation. Assimilation of NO_3^- results in isotopic fractionation with ε_{org-NO_3} between 0‰ and -10‰ in NO_3^- limited and NO_3^- replete conditions, respectively (Pennock et al., 1996). In dysoxic to anoxic environments, the removal of nitrogen from the marine system (NO_3^-, NH_4^+ and NO_2^- are converted into gaseous species NO_2 or N_2) takes place via denitrification and anammox, with large fractionations of ~ 20-30‰ in the water column, and negligible fractionation in the sediments (Sigman et al., 2009; Lam et al., 2009; Lam and Kuypers, 2011).

A recent compilation of published $\delta^{15}N$ values from the Yangtze Block documented modern-like $\delta^{15}N$ values during Cambrian Stage 3, implying that a large NO_3^- reservoir may have built up in well-oxygenated seawater during this time interval (Wang et al., 2018). Clearly, this is not consistent with the stratified ocean model suggested by the redox conditions documented across the Yangtze Block (e.g. Jin et al., 2016; Li et al., 2017). In order to better understand the prevailing redox structure and operation of the N cycle in the early Cambrian Yangtze ocean, we coupled inorganic redox proxies with $\delta^{15}N$ data from multiple sections across the Yangtze Block, as well as sections from the uplift margin close to the Cathaysia Block (Fig. 7; Table S3).

5.2.1 Late Cambrian Stage 2

During late Cambrian Stage 2, the majority of deep water sections (slope-basin) across the Yangtze Block show $\delta^{15}N$ values that range from -2 to 2‰ (Fig. 7), with a mean value close to the nitrogen isotopic composition of the atmosphere (0‰). Isotopic variability within this range can be explained by three possible mechanisms (see Stüeken, 2013 for detailed discussion): (i) Nitrogen fixation as the dominant pathway for nitrogen cycling, especially under anoxic conditions where nitrification (strictly dependent on O_2) is inhibited. Biological nitrogen fixation (reduction of N_2 to NH_4^+) with the most common Mo-based nitrogenase enzyme imparts a minimal isotopic fractionation of −1‰ on average, with a range from −2 to +1‰ (Zhang et al., 2014; Stüeken et al., 2016). This scenario is likely in the case of the Yangtze ocean during the late Cambrian Stage 2, because iron speciation data indicates that seawater was dominantly anoxic at depth (Fig. 5) and the sediments in this interval are characterized by high Mo concentrations (Scott et al., 2008; Chen et al., 2015). (ii) Fixed nitrogen is rapidly nitrified and then quantitatively denitrified due to the redox gradient in the water column.

Scenario (ii) is a possible explanation for the N isotope signals preserved at the shallowest water Xiaotan section, since intermittent oxic conditions occurred in the late Cambrian Stage 2. (iii) Under oxic conditions, fixed nitrogen is readily nitrified and denitrification is restricted to sediments. Scenario (iii) is unlikely because widespread anoxia has been well documented in this stage (e.g. Feng et al., 2014; Wang et al., 2015; Jin et al., 2016; Fig. 5). Thus, the biogeochemical pathway of the nitrogen cycle in the deep water during the late Cambrian Stage 2 was likely dominated by N_2 fixation (Fig. 8a).

Anomalous negative $\delta^{15}N$ values (< -2‰) are preserved in some samples from the outer-shelf Zhongnancun (Fig. 2) and Sancha sections, and also from the base of the inner-shelf CJ2 section (Fig. 7). Two alternative mechanisms can be considered to explain these negative $\delta^{15}N$ values: (i) N_2 fixation using alternative nitrogenases containing V or Fe as cofactors (instead of the more common Mo) can produce large isotopic fractionations of -6 to -8‰ (Zhang et al., 2014); (ii) non-quantitative NH_4^+ assimilation by organisms in NH_4^+ replete conditions could produce large fractionations of -4 to -27‰, depending on NH_4^+ concentrations (Pennock et al., 1996).

Scenario (i) has been invoked to explain the $\delta^{15}N$ values (-2 to -4‰) preserved in Cretaceous Oceanic Anoxic Event 2 (OAE-2) black shales, due to Mo-limited ocean anoxia (Zhang et al., 2014). However, this scenario seems unlikely, since even in the Mo-depleted, Fe-rich Precambrian oceans there is thus far no convincing evidence of biological N_2 fixation with V or Fe nitrogenases (Stüeken et al., 2013). Furthermore, this interpretation is also inconsistent with the high Mo concentration recorded in sediments during this period (Wang et al., 2015; Hammarlund et al., 2017; Scott et al., 2008; Chen et al., 2015). Scenario (ii) has been invoked to explain the negative $\delta^{15}N$ values (as low as -4‰) during Cretaceous OAE-2 (Higgins et al., 2012) and similar $\delta^{15}N$ values (as low as -4.7‰) in the late Paleoproterozoic (Papineau et al., 2009). This mechanism would be a reasonable interpretation for the low $\delta^{15}N$ values in this study (Fig. 8a), because the negative $\delta^{15}N$ values observed in shelf sections correspond well with euxinia (Fig. 7). Under euxinic conditions, the organic-bound NH_4^+ is likely to accumulate to high concentrations in the water column (review by Stüeken et al., 2016 for details).

Previous studies have suggested that partial NH_4^+ assimilation by anaerobic bacteria (e.g. green or purple sulfur bacteria) could result in these low $\delta^{15}N$ values in the early Cambrian Yangtze ocean during Cambrian Stage 2 (Wang et al., 2018). The NH_4^+ replete conditions may have built up in the shelf area due to strong upwelling of NH_4^+-rich anoxic waters from the deep ocean. These results are further consistent with a shallow chemocline and photic zone euxinia during the late Cambrian Stage 2. The majority of samples from shelf sections, however, preserve $\delta^{15}N$ values typical of nitrogen fixation (from -2 to 2‰), which may be attributable to the NH_4^+

transported from deep water being consumed quantitatively and thereby masking the fractionation associated with NH_4^+ assimilation.

5.2.2 Cambrian Stage 3

During the early-middle Cambrian Stage 3, widespread anoxic conditions existed in the Yangtze ocean (Figs 5 and 7). However, distinctive $\delta^{15}N$ values are preserved in different settings, with more positive values (generally between 0 and 3‰) recorded in the shelf environment and lower values (from -2 to 2‰) recorded in slope-basin settings (Figs. 7 and 9).

The positive shift in $\delta^{15}N$ values observed in sections from the inner-shelf and outer-shelf can be explained by three possible scenarios (Stüeken, 2013; Ader et al., 2016; Stüeken et al., 2016; Koehler et al., 2017): (i) Partial assimilation of NH_4^+ would preferentially consume isotopically light nitrogen and leave the residual NH_4^+ pool enriched in ^{15}N (Papineau et al., 2009); (ii) Partial nitrification of NH_4^+ can produce an isotopically light nitrate pool while leaving a residual NH_4^+ pool enriched in ^{15}N, because nitrification prefers lighter isotopes (Thomazo et al., 2011). Scenarios (i) and (ii) are unlikely explanations for the positive $\delta^{15}N$ shift in the shelf area of the early Cambrian Yangtze ocean for the following reasons. Firstly, mechanism (i) would result in two distinct isotopic facies, one which preserves low $\delta^{15}N$ values (<-2‰) and one which preserves high $\delta^{15}N$ values (>1‰). However, samples from the inner-shelf to the basin during this period do not record very negative $\delta^{15}N$ values. For example, the lowest $\delta^{15}N$ value from the slope (Longbizui) section is -2‰ and most values from deep water sections are close to 0‰, consistent with N_2 fixation (-2 to +2‰, Stüeken, 2013). Regarding scenario (ii), partial nitrification has so far been considered to occur only in marine environments that undergo transient seasonal changes, with no evidence for this process occurring over longer geologic timescales (Hadas et al., 2009; Granger et al., 2011). This leaves scenario (iii), whereby partial denitrification in the water column leaves the residual nitrate pool enriched in ^{15}N, because denitrification produces isotopically light nitrogenous gases, which removes ^{14}N from the system (e.g. Cline and Kaplan, 1975). Scenario (iii) is most likely in the case of the early Cambrian Yangtze ocean and nitrate appears to have been more abundant in shelf environment (Fig. 8b). This has also been considered as the main mechanism for the production of positive $\delta^{15}N$ values in the modern ocean (e.g. Lam et al., 2009; Tesdal et al., 2013) as well as in the early Cambrian Yangtze ocean (Hammarlund et al., 2017; Wang et al., 2018). These positive $\delta^{15}N$ excursion intervals have a good correspondence with ferruginous conditions, suggesting that the water column may also have experienced nitrogenous conditions. Oxygen is required for nitrification of ammonium to nitrate (Koehler et al., 2017), thereby higher nitrate levels in the shelf area suggest that oxic-suboxic conditions may have been established in shelf environment.

The $\delta^{15}N$ values (-2 to +2‰) of slope – basin sections during this period are similar to those in the late Cambrian Stage 2. The invariability of $\delta^{15}N$ values in these sections is consistent with the maintenance of anoxic and ferruginous conditions in deeper waters throughout Cambrian Stage 2 – 3 (Jin et al., 2016; Li et al., 2017), reflecting nitrogen limitation in slope – basin parts of the early Cambrian Yangtze ocean (Fig. 8b). However, the positive $\delta^{15}N$ excursions are found in the sections (Yanjia section, Chunye 1 drill core and Silikou section) close to the Cathaysia Block, and are interpreted to have resulted from denitrification (Wang et al., 2018; Zhang et al., 2018). These sections were considered to represent a deep water environment (Wang et al., 2018). Previous studies have suggested that at least the western Zhejiang area (where the Yanjia section and Chunye 1 drill core were located) was a semi-restricted gulf environment (Xue and Yu, 1979; Huang and Zhang, 1988; Xiang et al., 2018), and thus the nitrogen cycle here may have been different to that of the open ocean.

The $\delta^{15}N$ values preserved in all sections (Fig. 10) are, however, lower than the isotopic composition of modern oceanic sediments (+5‰, Tesdal et al., 2013). Lower $\delta^{15}N$ values documented in these sections can be explained by low oceanic dissolved oxygen and nitrate concentrations (Stüeken, 2013; Koehler et al., 2017). A small nitrate reservoir and low oxygen concentration in the water column would have decreased the nitrate inventory of the ocean without significantly increasing residual nitrate $\delta^{15}N$ values, thereby allowing preservation of a N isotopic signature characteristic of N_2 fixation (Stüeken, 2013; Ader et al., 2016; Kipp et al., 2018). It is noteworthy that the redox differences and latitude variations should also be taken into account when comparing ancient and modern oceans (e.g. Koehler et al., 2019). The $\delta^{15}N$ excursions observed in each of the shelf sections are of a similar magnitude (~3‰), which may imply that the $\delta^{15}N$ values in these sections could have recorded the values of the regional nitrate reservoir during the early Cambrian period, which was lower than that of the modern ocean. Although data from Yangtze basin cannot capture global trends in marine nitrogen cycling during early Cambrian and more data outside South China await further analysis and study here and elsewhere, it is possible that they may in part reflect a global phenomenon. This explanation is supported by long-term secular variation in the marine nitrogen cycle, suggesting that ^{15}N-depleted isotopic compositions in the Cambrian ocean were likely due to enhanced sedimentary denitrification, without significant nitrogen isotopic fractionation effects during greenhouse highstands (Algeo et al., 2014). Taken together, we conclude that the spatiotemporal distribution of $\delta^{15}N$ values, and the gradients in C and N isotopes (Fig. 9), suggest a stratified redox structure, consistent with that recorded by iron speciation and RSTE data.

5.3. Biological implications

During the late Cambrian Stage 2 to earliest Stage 3, continental margin environments such as the Yangtze Block, South China, exhibited variable degrees of anoxia and palaeoredox stratification. In such environments, negative carbonate carbon isotope excursions and low $\delta^{15}N$ values have been suggested to indicate periodic shoaling of the redoxcline into the photic zone (e.g. Wang et al., 2018; Chen et al., 2019). The extensive anoxia and intermittent photic zone euxinia, as confirmed by iron speciation and RSTE data, may have resulted in the extinction of small shelly fossils in early Cambrian oceans (Zhu et al., 2007; Wang et al., 2018).

The $\delta^{15}N$ gradient in the early Cambrian Yangtze ocean during early – middle Stage 3 (Fig. 9) is similar to the Mesoproterozoic Belt Supergroup (~ 1.4 billion years ago, Ga; Stüeken, 2013), and the Bangemall (~ 1.5 Ga) and Roper (~ 1.4 – 1.5 Ga) basins (Koehler et al., 2017), suggesting that the early Cambrian Yangtze ocean was characterized by generally low nitrate concentrations with a minimum in offshore deep water environments. It has been hypothesized that nitrogen availability may have played an important role in the evolutionary innovation of eukaryotes (Anbar and Knoll, 2002). If correct, the nitrate gradient may have restricted large-celled eukaryotes to near-shore environments, as in the case of the early evolution of eukaryotes in the Mesoproterozoic oceans (Stüeken, 2013; Koehler et al., 2017). The nitrate gradient observed in this study can be linked to fossil distributions in the early Cambrian Yangtze ocean, as demonstrated by Jin et al. (2016). These authors showed that the complexity of early animal ecosystems is spatially heterogeneous, with increased complexity in near-shore environments containing higher oxygen levels (Figs 5 and 7). The increased nitrogen availability in shelf environments may have enhanced the biological pump and the evolution of large-celled eukaryotic phytoplankton (Brocks et al., 2017; Wang et al., 2018). A corresponding increase in the size of organic particulates and faster sinking rates may have enhanced organic matter burial, thus reducing O_2 consumption in the water column and resulting in a positive feedback on further ocean oxygenation, and synchronized early animal radiations (Butterfield, 2009; Lenton et al., 2014).

Recently, He et al. (2019) documented a strong positive co-variation between carbonate $\delta^{13}C$ values and carbonate-associated sulfate $\delta^{34}S$ values in early Cambrian Siberian platform carbonates. The authors argued that this covariation records variability in atmospheric O_2 concentrations. Moreover, they suggest that episodic maxima in the biodiversity of animal phyla directly coincided with the extent of shallow-ocean oxygenation. Hammarlund et al. (2017) have shown that OMZ-type conditions persisted well into the interval characterized by the Chengjiang biota. However, the shallow shelf may have been dominantly well oxygenated at this time, providing a stable, oxygenated environment within which these energetically costly, motile lifestyles could have thrived.

When predatory animals, which produce larger fecal particulates, dominate the shallow water ecosystem, the sinking and burial of organic carbon is accelerated, thus reducing oxygen consumption in the water column and allowing oxygen to reach deeper waters (Logan et al., 1995). Furthermore, sponges, which dominate the deep water ecosystem of the early Cambrian Yangtze ocean (Zhu, 2010; Fig. 5), may have also played a role in the accumulation of oxygen in the deep waters by filtering the reduced carbon in the water column (Lenton et al., 2014). The appearance of macrozooplankton (i.e. bivalved arthropod *Isoxys*) and suspension-feeding mesozooplankton (i.e. anomalocarid *Tamisiocaris borealis*) in Cambrian Stage 3 (Luo et al., 1994; Vinther et al., 2014) provides reliable paleontological evidence for this hypothesis. Although global Fe speciation data suggest that deep waters remained largely anoxic in some basins during Cambrian Stage 3 (Sperling et al., 2015; Li et al., 2017), oxic conditions (Fig. 5), and a transition from abundant sponge spicules to articulated sponges (Wang et al., 2012; Jin et al., 2016) observed at the deep water Longbizui section, may provide evidence for at least local ventilation of deep water settings (slope-basin) during Cambrian Stage 4 in South China. Furthermore, OMZ-type stratification with at least weakly oxygenated deeper waters has recently been recorded from detailed regional paleoredox assessments of lower Cambrian sediments of the Baltic Basin (Guilbaud et al., 2018), and South China (Hammarlund et al., 2017) raising the possibility for widespread restructuring of the paleoredox landscape by Cambrian Stage 4.

6. Conclusions

Multi-proxy geochemical data are reported for the outer-shelf Zhongnancun section of the early Cambrian Yangtze Block in South China. Results reveal that the redox conditions progressively evolved from euxinic, through ferruginous, to oxic during deposition of the Niutitang Formation. Our new data combined with existing data from the shelf to the basin environment, suggest that during Cambrian stages 2 – 3, the Yangtze ocean was redox stratified with euxinic mid-depths dynamically maintained between oxic surface waters and ferruginous deeper waters. However, by early Cambrian Stage 4 (~514 Ma), deep waters may have become intermittently oxygenated.

Nitrogen isotope data from successions across the Yangtze Block show that, during late Cambrian Stage 2, N_2 fixation was the dominant biogeochemical pathway of the nitrogen cycle. Anomalously light $\delta^{15}N$ values (<-2‰) observed in shelf sections correspond well with euxinia, suggesting that partial assimilation of NH_4^+ was the dominant pathway for nitrogen cycling in euxinic waters, and NH_4^+ may have built up to high concentrations.

During early – middle Cambrian Stage 3, a distinct gradient in $\delta^{15}N$ is observed in the early Cambrian Yangtze ocean, with more positive values (between 0 and 3‰) recorded in shelf sections and lighter values (from -2 to 2‰) recorded in slope-basin sections. The positive shift in $\delta^{15}N$ values preserved in the shelf sections likely results from partial denitrification in the water column, while $\delta^{15}N$ values of ~0‰, recorded in deeper water sections may have resulted from N_2 fixation. The $\delta^{15}N$ values preserved in all sections are lower than those of the modern ocean, indicating that the early Cambrian

Yangtze ocean may be characterized by low nitrate concentrations. Furthermore, the spatiotemporal distribution of the $\delta^{15}N$ values, together with the stratigraphic gradients in C and N isotopes, and Fe speciation data, are all consistent with a model of, at least, regional-scale palaeo-marine redox stratification.

The $\delta^{15}N$ gradient in the early Cambrian Yangtze ocean is similar to that suggested for Mesoproterozoic oceans (Stüeken, 2013; Koehler et al., 2017), implying that nitrate was limited in offshore environments, restricting eukaryotes to near-shore environments. Increased nitrogen availability in shelf environments would have enhanced the biological pump and the evolution of large-celled eukaryotic phytoplankton, which may have produced a positive feedback on further ocean oxygenation, allowing for increased complexity and diversity of early animal ecosystems on oxic shelves.

Acknowledgments

This work was supported by the National Science and Technology Major Project (Grant No. 2016ZX05034-002-001), National Natural Science Foundation of China (Grant No. 41927801), Fundamental Research Funds for the Central Universities (Grant No. 2652019098), the Helmholtz-Rekrutierungsinitive (SG and JM), SWP and FTB were funded by NERC (NE/R010129/1), and SWP acknowledges support from a Royal

Society Wolfson Research Merit Award. We thank the editor in chief Michael E. Böttcher and two reviewers (Eva E. Stüeken and Matthew C. Koehler) for their comments that significantly improved this paper.

References

Ader, M., Thomazo, C., Sansjofre, P., Busigny, V., Papineau, D., Laffont, R., Cartigny, P., Halverson, G.P., 2016. Interpretation of the nitrogen isotopic composition of Precambrian sedimentary rocks: assumptions and perspectives. Chem. Geol. 429, 93-110.

Algeo, T., Rowe, H., Hower, J.C., Schwark, L., Herrmann, A., Heckel, P., 2008. Changes in ocean denitrification during Late Carboniferous glacial–interglacial cycles. Nat.Geosci. 1, 709-714.

Algeo, T.J., Lyons, T.W., 2006. Mo-total organic carbon covariation in modern anoxic marine environments: implications for analysis of paleoredox and paleohydrographic conditions. Paleoceanography 21, PA1016.

Algeo, T.J., Meyers, P.A., Robinson, R.S., Rowe, H., Jiang, G.Q., 2014. Icehouse-greenhouse variations in marine denitrification. Biogeosciences 11, 1273-1295.

Algeo, T.J., Rowe, H., 2012. Paleoceanographic applications of trace-metal concentration data. Chem. Geol. 324, 6-18.

Algeo, T.J., Tribovillard, N., 2009. Environmental analysis of paleoceanographic systems based on molybdenum-uranium covariation. Chem. Geol. 268, 211-225.

Anbar, A., Duan, Y., Lyons, T.W., Arnold, G.L., Kendall, B., Creaser, R.A., Kaufman, A.J., Gordon, G.W., Scott, C.T., Garvin, J., Buick, R., 2007. A whiff of oxygen before the Great Oxidation Event? Science 317 (5846), 1903-1906.

Anbar, A.D., Knoll, A.H., 2002. Proterozoic ocean chemistry and evolution: a bioinorganic bridge? Science 297, 1137-1142.

Bowyer, F., Wood, R.A., Poulton, S.M., 2017. Controls on the evolution of Ediacaran metazoan ecosystems: A redox perspective. Geobiology 00, 1-36.

Brocks, J.J., Jarrett, A.J.M., Sirantoine, E., Hallmann, C., Hoshino, Y., Liyanage, T., 2017. The rise of algae in Cryogenian oceans and the emergence of animals. Nature 548, 578-581.

Butterfield, N.J., 2009. Oxygen, animals and oceanic ventilation: an alternative view. Geobiology 7, 1-7.

Campbell, I.H., Squire, R.J., 2010. The mountains that triggered the Late Neoproterozoic increase in oxygen: The Second Great Oxidation Event. Geochim. Cosmochim. Acta 74, 4187-4206.

Canfield, D.E., Thamdrup, B., 2009. Towards a consistent classification scheme for geochemical environments, or, why we wish the term ‘suboxic’ would go away. Geobiology 7, 385-392.

Canfield, D.E., Glazer, A.N., Falkowski, P.G., 2010. The evolution and future of Earth’s nitrogen cycle. Science 330, 192-196.

Canfield, D.E., Poulton, S.W., Knoll, A.H., Narbonne, G.M., Ross, G., Goldberg, T., Strauss, H., 2008. Ferruginous conditions dominated later Neoproterozoic deep-water chemistry. Science 321, 949-952.

Canfield, D.E., Poulton, S.W., Narbonne, G.M., 2007. Late-Neoproterozoic deep-ocean oxygenation and the rise of animal life. Science 315, 92-95.

Canfield, D.E., Raiswell, R., Westrich, J.T., Reaves, C.M., Berner, R.A., 1986. The use of chromium reduction in the analysis of reduced inorganic sulfur in sediments and shales. Chem. Geol. 54, 149-155.

Chen, X., Ling, H.-F., Vance, D., Shields-Zhou, G.A., Zhu, M., Poulton, S.W., Och, L.M., Jiang, S.Y., Li, D., Cremonese, L., Archer, C., 2015. Rise to modern levels of ocean oxygenation coincided with the Cambrian radiation of animals. Nat. Commun. 6.

Chen, Y., Diamond, C.W., Stüeken, E.E., Cai, C.F., Gill, B.C., Zhang, F.F., Bates, S.M., Chu, X.L., Ding, Y., Lyons, T.W., 2019. Coupled evolution of nitrogen cycling and redoxcline dynamics on the Yangtze Block across the Ediacaran-Cambrian transition. Geochim. Cosmochim. Acta 257, 243-265.

Clarkson, M.O., Poulton, S.W., Guilbaud, R., Wood, R.A., 2014. Assessing the utility of Fe/Al and Fe-speciation to record water column redox conditions in carbonate-rich sediments. Chem. Geol. 382, 111-122.

Cline, J.D., Kaplan, I.R., 1975. Isotopic fractionation of dissolved nitrate during denitrification in the eastern tropical North Pacific. Mar. Chem. 3, 271-299.

Cremonese, L., Shields-Zhou, G., Struck, U., Ling, H.F., Och, L., Chen, X., Li, D., 2013. Marine biogeochemical cycling during the early Cambrian constrained by a nitrogen and organic carbon isotope study of the Xiaotan section, South China. Precambrian Res. 225, 148-165.

Cremonese, L., Shields-Zhou, G.A., Struck, U., Ling, H.-F., Och, L.M., 2014. Nitrogen and organic carbon isotope stratigraphy of the Yangtze Platform during the Ediacaran-Cambrian transition in South China. Palaeogeogr. Palaeoclimatol. Palaeoecol. 398, 165-186.

Doyle, K.A., Poulton, S.W., Newton, R.J., Podkovyrov, V.N., Bekker, A., 2018. Shallow water anoxia in the Mesoproterozoic ocean: Evidence from the Bashkir Meganticlinorium, Southern Urals. Precambrian Res. 317, 196-210.

Feng, L., Li, C., Huang, J., Chang, H., Chu, X., 2014. A sulfate control on marine mid-depth euxinia on the early Cambrian (ca. 529-521 Ma) Yangtze platform, South China. Precambrian Res. 246, 123-133.

Gao, P., Liu, G., Jia, C., Ding, X., Chen, Z., Dong, Y., Zhao, X., Jiao, W., 2015. Evaluating rare earth elements as a proxy for oil–source correlation. A case study from Aer Sag, Erlian Basin, Northern China. Org. Geochem. 87, 35-54.

Gao, P., Li, S., Lash, G.G., He, Z., Xiao, X., Zhang, D., Hao, Y., 2020. Silicification and Si cycling in a silica-rich ocean during the Ediacaran-Cambrian transition. Chem. Geol. 119787.

Godfrey, L.V., Falkowski, P.G., 2009. The cycling and redox state of nitrogen in the Archaean ocean. Nat. Geosci. 2, 725-729.

Godfrey, L.V., Poulton, S.W., Bebout, G.E., Fralick, P.W., 2013. Stability of the nitrogen cycle during development of sulfidic water in the redox-stratified late Paleoproterozoic ocean. Geology 41, 655-658.

Goldberg, T., Strauss, H., Guo, Q., Liu, C., 2007. Reconstructing marine redox conditions for the Early Cambrian Yangtze Platform: evidence from biogenic sulphur and organic carbon isotopes. Palaeogeogr. Palaeoclimatol. Palaeoecol. 254, 175-193.

Granger, J., Sigman, D.M., Lehmann, M.F., Tortell, P.D., 2008. Nitrogen and oxygen isotope fractionation during dissimilatory nitrate reduction by denitrifying bacteria. Limnol. Oceanogr. 53, 2533-2545.

Guilbaud, R., Slater, B.J., Poulton, S.W., Harvey, T.H.P., Brocks, J.J., Nettersheim, B.J., Butterfield, N.J., 2018. Oxygen minimum zones in the early Cambrian ocean. Geochem. Persp. Let. 6, 33-38.

Hadas, O., Altabet, M.A., Agnihotri, R., 2009. Seasonally varying nitrogen isotope biogeochemistry of particulate organic matter (POM) in Lake Kinneret, Israel. Limnol. Oceanogr. 54, 75-85.

Hammarlund, E.U., Gaines, R.R., Prokopenko, M.G., Qi, C., Hou, X.G., Canfield, D.E., 2017. Early Cambrian oxygen minimum zone-like conditions at Chengjiang. Earth Planet. Sci. Lett. 475, 160-168.

He, T., Zhu, M., Mills, B.J.W., Wynn, P.M., Zhuravlev, A.Y., Tostevin, R., Pogge von Strandmann, P.A.E., Yang, A., Poulton, S.W., Shields, G.A., 2019. Possible links between extreme oxygen perturbations and the Cambrian radiation of animals. Nat. Geosci. 12, 468-474.

Higgins, M.B., Robinson, R.S., Husson, J.M., Carter, S.J., Pearson, A., 2012. Dominant eukaryotic export production during ocean anoxic events reflects the importance of recycled NH^{4+}. Proc. Natl. Acad. Sci. U. S. A. 109, 2269-2274.

Huang, Z.H., Zhang, S.W., 1988. Lithofacies paleogeography of Cambrian Zhejiang Province. Lithofacies Paleogeogr. 33, 13-21 (in Chinese).

Jiang, G.Q., Wang, X.Q., Shi, X.Y., Xiao, S.H., Zhang, S.H., Dong, J., 2012. The origin of decoupled carbonate and organic carbon isotope signatures in the early Cambrian (ca. 542-520 Ma) Yangtze platform. Earth Planet. Sci. Lett. 317, 96-110.

Jiang, S.Y., Chen, Y.Q., Ling, H.F., Yang, J.H., Feng, H.Z., Ni, P., 2006. Trace-and rare-earth element geochemistry and Pb-Pb dating of black shales and intercalated Ni-Mo-PGE-Au sulfide ores in Lower Cambrian strata, Yangtze Platform, South China. Miner. Depos. 41, 453-467.

Jiang, S.Y., Pi, D.H., Heubeck, C., Frimmel, H., Liu, Y.P., Deng, H.L., Ling, H.F., Yang, J.H., 2009. Early Cambrian ocean anoxia in south China.

Nature 459, E5-E6.

Jin, C., Li, C., Algeo, T.J., Planavsky, N.J., Cui, H., Yang, X., Zhao, Y., Zhang, X., Xie, S., 2016. A highly redox-heterogeneous ocean in South China during the early Cambrian (~529-514 Ma): implications for biota-environment co-evolution. Earth Planet. Sci. Lett. 441, 38-51.

Kipp, M.A., Stüeken, E.E., Yun, M., Bekker, A., Buick, R., 2018. Pervasive aerobic nitrogen cycling in the surface ocean across the Paleoproterozoic Era. Earth Planet. Sci. Lett. 500, 117-126.

Kříbek, B., Sýkorová, I., Pašava, J., Machovič, V., 2007. Organic geochemistry and petrology of barren and Mo-Ni-PGE mineralized marine black shales of the Lower Cambrian Niutitang Formation (South China). Int. J. Coal Geol. 72, 240-256.

Koehler, M.C., Stüeken, E.E., Hillier, S., Prave, A.R., 2019. Limitation of fixed nitrogen and deepening of the carbonate-compensation depth through the Hirnantian at Dob's Linn, Scotland. Palaeogeogr. Palaeoclimatol. Palaeoecol. 534, 109321.

Koehler, M.C., Stüeken, E.E., Kipp, M.A., Buick, R., Knoll, A.H., 2017. Spatial and temporal trends in Precambrian nitrogen cycling: a Mesoproterozoic offshore nitrate minimum. Geochim. Cosmochim. Acta 198, 315-337.

Krause, A.J., Mills, B.J.W., Zhang, S, Planavsky, N.J., Lenton, T.M., Poulton, S.W., 2018. Stepwise oxygenation of the Paleozoic atmosphere. Nat. Commun. 9, 4081.

Lam, P., Lavik, G., Jensen, M.M., van de Vossenberg, J., Schmid, M., Woebken, D., Dimitri Gutiérrez, D., Amann, R., Jetten, M.S.M., Kuypers, M.M.M., 2009. Revising the nitrogen cycle in the Peruvian oxygen minimum zone. Proc. Natl. Acad. Sci. U. S. A. 106, 4752-4757.

Lehmann, B., Nägler, T.F., Holland, H.D., Wille, M., Mao, J.W., Pan, J.Y., Ma, D.S., Dulski, P., 2007. Highly metalliferous carbonaceous shale and Early Cambrian seawater. Geology 35, 403-406.

Lenton, T.M., Boyle, R.A., Poulton, S.W., Shields-Zhou, G.A., Butterfield, N.J., 2014. Co-evolution of eukaryotes and ocean oxygenation in the Neoproterozoic era. Nature Geosci. 7, 257-265.

Li C., Jin C., Planavsky N. J., Algeo T. J., Cheng M., Yang X., Zhao Y., Xie S., 2017. Coupled oceanic oxygenation and metazoan diversification during the early-middle Cambrian? Geology 45, 743-746.

Li, C., Cheng, M., Zhu, M., Lyons, T.W., 2018. Heterogeneous and dynamic marine shelf oxygenation and coupled early animal evolution. Emerg. Top. Life. Sci. 28, 279-288.

Li, C., Love, G.D., Lyons, T.W., Fike, D.A., Sessions, A.L., Chu, X., 2010. A stratified redox model for the Ediacaran ocean. Science 328, 80-83.

Logan, G.A., Hayes, J., Hieshima, G.B., Summons, R.E., 1995. Terminal Proterozoic re-organization of biogeochemical cycles. Nature 376, 53-56.

Luo, H.L., Jiang, Z.W., Tang, L.D., 1994. Stratotype Section for Lower Cambrian Stages in China. Yunnan Science and Technology Press, Kunming, China (in Chinese with English abstract).

Magnall, J.M., Gleeson, S.A., Poulton, S.W., Gordon, G.W., Paradis, S., 2018. Links between seawater paleoredox and the formation of sediment-hosted massive sulphide (SHMS) deposits-Fe speciation and Mo isotope constraints from Late Devonian mudstones. Chem. Geol. 490, 45-60.

McLennan, S.M., 2001. Relationships between the trace element composition of sedimentary rocks and upper continental crust. Geochemistry, Geophysics, Geosystems 2, paper number 2000GC000109.

Merdith, A.S., Collins, A.S., Williams, S.E., Pisarevsky, S., Foden, J.F., Archibald, D.A., Blades, M.L., Alessio, B.L., Armistead, S., Plavsa, D., Clark, C., Müller, R.D., 2017. A full-plate global reconstruction of the Neoproterozoic. Gondwana Res. 50, 84-134.

Och, L.M., Cremonese, L., Shields-Zhou, G.A., Poulton, S.W., Struck, U., Ling, H., Li, D., Chen, X., Manning, C., Thirlwall, M., Strauss, H., Zhu, M., 2016. Palaeoceanographic controls on spatial redox distribution over the Yangtze Platform during the Ediacaran–Cambrian transition. Sedimentology. 63, 378-410.

Och, L.M., Shields-Zhou, G.A., Poulton, S.W., Manning, C., Thirlwall, M.F., Li, D., Chen, X., Ling, H., Osborn, T., Cremonese, L., 2013. Redox changes in Early Cambrian black shales at Xiaotan section, Yunnan Province, South China. Precambrian Res. 225, 166-189.

Papineau, D., Purohit, R., Goldberg, T., Pi, D., Shields, G.A., Bhu, H., Steele, A., Fogel, M.L., 2009. High primary productivity and nitrogen cycling after the Paleoproterozoic phosphogenic event in the Aravalli supergroup, India. Precambrian Res. 171, 37-56.

Pennock, J.R., Velinsky, D.J., Ludlam, J.M., Sharp, J.H., Fogel, M.L., 1996. Isotopic fractionation of ammoniumand nitrate during uptake by Skeletonema costatum: implications for $\delta^{15}N$ dynamics under bloom conditions. Limnol. Oceanogr. 41, 451-459.

Pi, D.H., Liu, C.Q., Shields-Zhou, G.A., Jiang, S.Y., 2013. Trace and rare earth element geochemistry of black shale and kerogen in the early Cambrian Niutitang Formation in Guizhou province, South China: constraints for redox environments and origin of metal enrichments. Precambr. Res. 225, 218-229.

Poulton, S.W., Canfield, D.E., 2005. Development of a sequential extraction procedure for iron: implications for iron partitioning in continentally derived particulates. Chem. Geol. 214, 209-221.

Poulton, S.W., Canfield, D.E., 2011. Ferruginous conditions: a dominant feature of the ocean through Earth's history. Elements 7, 107-112.

Poulton, S.W., Fralick, P.W., Canfield, D.E., 2010. Spatial variability in oceanic redox structure 1.8 billion years ago. Nat. Geosci. 3, 486-490.

Poulton, S.W., Fralick, P.W., Canfield, D.E., 2004. The transition to a sulphidic ocean approximately 1.84 billion years ago. Nature 431, 173-177.

Poulton, S.W., Raiswell, R., 2002. The low-temperature geochemical cycle of iron: from continental fluxes to marine sediment deposition. Am. J. Sci. 302, 774-805.

Raiswell, R., Canfield, D.E., 2012. The iron biogeochemical cycle past and present. Geochem. Persp. 1, 1-220.

Raiswell, R., Hardisty, D.S., Lyons, T.W., Canfield, D.E., Owens, J.D., Planavsky, N.J., Poulton, S.W., Reinhard, C.T., 2018. The iron paleoredox proxies: a guide to the pitfalls, problems and proper practice. Am. J. Sci. 318, 491-526.

Sahoo, S.K., Planavsky, N.J., Kendall, B., Wang, X.Q., Shi, X.Y., Scott, C., Anbar, A.D., Lyons, T.W., Jiang, G.Q., 2012. Ocean oxygenation in the wake of the Marinoan glaciation. Nature 489, 546-549.

Scholz, F., McManus, J., Sommer, S., 2013. The manganese and iron shuttle in a modern euxinic basin and implications for molybdenum cycling at euxinic ocean margins. Chem. Geol. 355, 56-68.

Scott, C., Lyons, T. W., Bekker, A., Shen, Y., Poulton, S. W., Chu, X., Anbar, A. D., 2008. Tracing the stepwise oxygenation of the Proterozoic ocean. Nature 452, 456-459.

Scott, C., Lyons, T.W., 2012. Contrasting molybdenum cycling and isotopic properties in euxinic versus non-euxinic sediments and sedimentary rocks: refining the paleoproxies. Chem. Geol. 324, 19-27.

Sperling, E.A., Wolock, C.J., Morgan, A.S., Gill, B.C., Kunzmann, M., Halverson, G.P., Macdonald, F.A., Knoll, A.H., Johnston, D.T., 2015. Statistical analysis of iron geochemical data suggests limited late Proterozoic oxygenation. Nature 523, 451-454.

Steiner, M., Wallis, E., Erdtmann, B.D., Zhao, Y.L., Yang, R.D., 2001. Submarine-hydrothermal exhalative ore layers in black shales from South China and associated fossils-insights into a Lower Cambrian facies and bio-evolution. Palaeogeogr. Palaeoclimatol. Palaeoecol. 169, 165-191.

Stüeken, E.E., 2013. A test of the nitrogen-limitation hypothesis for retarded eukaryote radiation: nitrogen isotopes across a Mesoproterozoic basinal profile. Geochim. Cosmochim. Acta 120, 121-139.

Stüeken, E.E., Kipp, M.A., Koehler, M.C., Buick, R., 2016. The evolution of earth's biogeochemical nitrogen cycle. Earth Sci. Rev. 160, 220-239.

Tesdal, J.E., Galbraith, E.D., Kienast, M., 2013. Nitrogen isotopes in bulk marine sediment: linking seafloor observations with subseafloor records. Biogeosciences 10, 101-118.

Thomazo, C., Ader, M., Phillippot, P., 2011. Extreme ^{15}N enrichment in 2.72-Gyr-old sediments: evidence for a turning point in the nitrogen cycle. Geobiology 9, 107-120.

Tostevin, R., Wood, R.A., Shields, G.A., Poulton, S.W., Guilbaud, R., Bowyer, F., Penny, A.M., He, T., Curtis, A., Hoffmann, K.H., Clarkson, M.O., 2016.

Low-oxygen waters limited habitable space for early animals. Nat. Commun. 7, 12818.

Tribovillard, N., Algeo, T.J., Lyons, T., Riboulleau, A., 2006. Trace metals as paleoredox and paleoproductivity proxies: an update. Chem. Geol. 232, 12-32.

Vinther, J., Stein, M., Longrich, N.R., Harper, D.A.T., 2014. A suspension-feeding anomalocarid from the Early Cambrian. Nature 507, 496-499.

Wang, D., Ling, H.F., Struck, U., Zhu, X.K., Zhu, M., He, T., Yang, B., Gamper, A., Shields G. A., 2018. Coupling of ocean redox and animal evolution during the Ediacaran-Cambrian transition. Nat. Commun. 9, 2575.

Wang, D., Struckb, U., Ling, H.F., Guo, Q.J., Graham, A., Zhou, S., Zhu, M.Y., Yao, S.P., 2015. Marine redox variations and nitrogen cycle of the early Cambrian southern margin of the Yangtze Platform, South China: evidence from nitrogen and organic carbon isotopes. Precambrian Res. 267, 209-226.

Wang, J., Chen, D., Yan, D., Wei, H., Xiang, L., 2012. Evolution from an anoxic to oxic deep ocean during the Ediacaran-Cambrian transition and implications for bioradiation. Chem. Geol. 306-307, 129-138.

Wen, H. J., Fan, H. F., Zhang, Y. X., Cloquet, C., Carignan, J., 2015. Reconstruction of early Cambrian ocean chemistry from Mo isotopes. Geochim. Cosmochim. Acta 164, 1-16.

Wille, M., Nägler, T.F., Lehmann, B., Schröder, S., Kramers, J.D., 2008. Hydrogen sulphide release to surface waters at the Precambrian/Cambrian boundary. Nature 453, 767-769.

Wood, R., Liu, A.G., Bowyer, F., Wilby, P.R., Dunn, F.S., Kenchington, C.G., Cuthill, J.F.H., Mitchell, E.G., Penny, A., 2019. Integrated records of environmental change and evolution challenge the Cambrian Explosion. Nat. Ecol. Evol. 3, 528-538.

Xiang, L., Schoepfer, S.D., Zhang, H., Cao, C.Q., Shen, S.Z., 2018. Evolution of primary producers and productivity across the Ediacaran-Cambrian transition. Precambrian Res. 313, 68-77.

Xu, D.T., Wang, X.Q., Shi, X.Y., Tang, D.J., Zhao, X.K., Feng, L.J., Song, H.Y., 2020. Nitrogen cycle perturbations linked to metazoan diversification during the early Cambrian. Palaeogeogr. Palaeoclimatol. Palaeoecol. 538, 109392.

Xu, L.G., Lehmann, B., Mao, J.W., Nägler, T.F., Neubert, N., Böttcher, M.E., Escher, P., 2012. Mo isotope and trace element patterns of Lower Cambrian black shales in South China: multi-proxy constraints on the paleoenvironment. Chem. Geol. 318-319, 45-59.

Xu, L.G., Lehmann, B., Mao, J.W., Qu, W.J., Du, A.D., 2011. Re-Os age of polymetallic Ni–Mo–PGE-Au mineralization in early Cambrian black shales of South China-a reassessment. Econ. Geol. 106, 511-522.

Xue, Y.S., Yu, C.L., 1979. Petrology and depositional environment analysis of

Hetang Formation, Lower Cambrian, western Zhejiang and eastern Jiangxi. Acta Stratigraphica Sin. 3, 283-295 (in Chinese).

Yin, R., Xu, L., Lehmann, B., Lepak, R.F., Hurley, J.P., Mao, J.W., Feng, X., Hu, R., 2017. Anomalous mercury enrichment in Early Cambrian black shales of South China: Mercury isotopes indicate a seawater source. Chem. Geol. 467, 159-167.

Zerkle, A.L., Poulton, S.W., Newton, R.J, Mettam, C., Claire, M.W., Bekker, A., Junium, C.K., 2017. Onset of the aerobic nitrogen cycle during the Great Oxidation Event. Nature 542, 392-512

Zhang, J., Fan, T., Zhang, Y., Lash, G.G., Li, Y., Wu, Y., 2017. Heterogenous oceanic redox conditions through the Ediacaran-Cambrian boundary limited the metazoan zonation. Sci. Rep. 7, 8550.

Zhang, X., Sigman, D.M., Morel, F.M., Kraepiel, A.M., 2014. Nitrogen isotope fractionation by alternative nitrogenases and past ocean anoxia. Proc. Natl. Acad. Sci. 111, 4782-4787.

Zhang, Z., Li, C., Cheng, M., Algeo, T. J., Jin, C., Tang, F., Huang, J., 2018. Evidence for highly complex redox conditions and strong water-column stratification in an early Cambrian continental-margin sea. Geochemistry, Geophysics, Geosystems, 19, 2397-2410.

Zhu, M., Strauss, H., Shields, G.A., 2007. From snowball earth to the Cambrian bioradiation: calibration of Ediacaran-Cambrian earth history in South China. Palaeogeogr. Palaeoclimatol. Palaeoecol. 254, 1-6.

Zhu, M.Y., 2010. The origin and Cambrian explosion of animals: Fossil evidence from China. Acta Palaeontol. Sin. 49, 269-287 (in Chinese with English abstract).

Zhuravlev, A. Yu., Wood, R. A., 1996. Anoxia as the cause of the mid-Early Cambrian (Botomian) extinction event. Geology. 24, 311-314.

Figure captions

Fig. 1, Simplified geological map of the Yangtze Platform (after Steiner et al., 2001; Jiang et al., 2012) and stratigraphic column of outer-shelf Zhongnancun section. Sections: 1-Xiaotan, 2-Meishucun, 3-CJ2 drill core, 4-Jinsha, 5-Dingtai, 6-Zhongnancun, 7-Sancha, 8-Yangjiaping, 9-Wengan, 10-Songtao, 11-Longbizui, 12-zk2012 drill core, 13-Lijiatuo, 14-Yuanjia, 15-Siduping, 16-Hejiapu, 17-Silikou, 18-Yanjia, 19-Chunye 1 drill core.

Fig. 2, Stratigraphic distribution of Fe species, TOC contents, TN contents, Mo, U and V concentrations, Mo/TOC ratios, $\delta^{13}C_{org}$ and $\delta^{15}N_{sed}$ values at the Zhongnancun section (reference $\delta^{15}N_{sed}$ data at the Zhongnancun section from Zhang et al., 2017 with orange symbol). Gray vertical lines represent the divisions between oxic (Fe_{HR}/Fe_T < 0.22; Poulton and Raiswell, 2002), equivocal (Fe_{HR}/Fe_T = 0.22-0.38; Poulton and Canfield, 2011) and anoxic conditions (Fe_{HR}/Fe_T > 0.38; Poulton and Raiswell, 2002), and between ferruginous and euxinic conditions (Fe_{py}/Fe_{HR}=0.7; Poulton and Canfield, 2011).

Fig. 3, Crossplot of Mo versus TOC (a) and U versus TOC. A good positive correlation of Mo and TOC content can be found in samples from Interval 3, but the lack of correlation between Mo and TOC for Interval 1 and 2 suggests that the black shales with higher Mo contents from Interval 1 and 2 are deposited in euxinic/anoxic environments and the black shales with low Mo concentration from Interval 3 are deposited in oxic/suboxic environments. The content of U and TOC decreased gradually from Interval 1 to Interval 3 and the U-TOC correlation becomes stronger, suggesting that the redox condition evolved from euxinic to oxic/suboxic.

Fig. 4, Crossplots of Mo_{EF} versus U_{EF} with enrichment factors normalized to AUCC (McLennan, 2001). The trend lines are modified from Algeo and Tribovillard (2009). The data includes the section of this study and the compiled data from multiple sections (CJ2 from Hammarlund et al., 2017, Jinsha and Wengan from Jin et al., 2016, Dingtai from Xu et al., 2012), all of the data correspond to the Cambrian Stage 2 to 3.

Fig. 5, Spatio-temporal variations in watermass redox conditions from inner-shelf to basin environment. The redox conditions of Xiaotan (Och et al., 2013), CJ2 drill core (Hammarlund et al., 2017), Jinsha (Jin et al., 2016), Wengan (Jin et al., 2016), Songtao (Goldberg et al., 2007; Guo et al., 2007; Canfield et al., 2008), Longbizui (Wang et al., 2012), Silikou (Zhang et al., 2018), Chunye1 drill core (Xiang et al., 2018) sections are reconstructed from Fe speciation data; the redox conditions of Sancha and Yuanjia are reconstructed from $\delta^{13}C_{org}$, $\delta^{15}N_{sed}$ and Mo data (Wang et al., 2015).

Fig. 6, The biogeochemical nitrogen cycle. Elements in parentheses are used as co-factors in enzymes and ε is the fractionation factor (‰) related to the metabolic process ($\varepsilon \approx \delta^{15}N_{product} - \delta^{15}N_{reactant}$). Adapted from Stüeken et al. (2016).

Fig. 7, Nitrogen isotope chemostratigraphy of Xiaotan section (Cremonese et al., 2013), CJ2 drill core (Hammarlund et al., 2017), Zhongnancun section (this study), Sancha section (Wang et al., 2015), Siduping and Hejiapu sections (Xu et al., 2020), Longbizui section (Cremonese et al., 2014), zk2012 drill core (Chen et al., 2019), Lijiatuo section (Cremonese et al., 2014), Yuanjia section (Wang et al., 2015), Silikou section (Zhang et al., 2018), Yanjia section (Wang et al., 2018) and Chunye1 drill core (Xiang et al., 2018).

Fig. 8, Schematic of the proposed nitrogen cycle in the early Cambrian Yangtze ocean during late Stage 2 (a) and early-middle Stage 3 (b).

Fig. 9, $\delta^{15}N_{sed}$ plotted against $\delta^{13}C_{org}$ for the multiple sections in the Yangtze Block, the plot only includes those samples corresponding to anoxic conditions during the early-middle Cambrian Stage 3. The data of shelf sections include Xiaotan section (Cremonese et al., 2013), CJ2 drill core (Hammarlund et al., 2017), Zhongnancun section (this study) and Sancha section (Wang et al., 2015). The data of slope-basin sections include Siduping and Hejiapu sections (Xu et al., 2020), Longbizui section (Cremonese et al., 2014), zk2012 drill core (Chen et al., 2019), Lijiatuo section (Cremonese et al., 2014) and Yuanjia section (Wang et al., 2015).

Fig. 10, Nitrogen isotope distributions of modern surface sediments (Testal et al., 2013) and early Cambrian Yangtze Block, South China (ca. 521-514 Ma).

Table captions

Table S1: Geochemical data for studied samples from Niutitang Formation at Zhongnancun section, South China.

Table S2: Fe speciation data for early Cambrian successions in the Yangtze Block.

Table S3: $\delta^{15}N$ and $\delta^{13}C_{org}$ values for early Cambrian successions in the Yangtze Block.

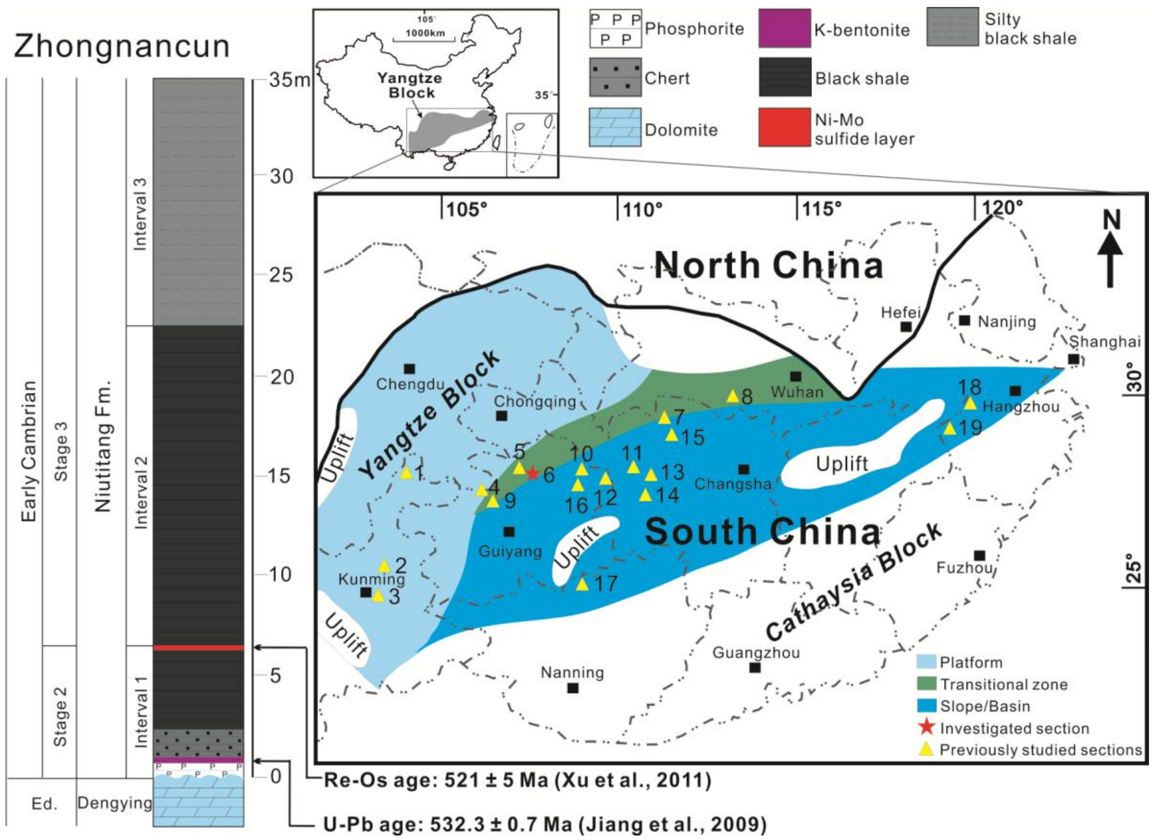
Zhongnancun
35m
30
25
20
15
10
5
0
Early Cambrian
Stage 3
Stage 2
Niutitang Fm.
Interval 3
Interval 2
Interval 1
Ed.
Dengying
Re-Os age: 521 ± 5 Ma (Xu et al., 2011)
U-Pb age: 532.3 ± 0.7 Ma (Jiang et al., 2009)
Yangtze Block
1000km
Phosphorite
Chert
Dolomite
K-bentonite
Black shale
Ni-Mo sulfide layer
Silty black shale
105°
110°
115°
120°
30°
25°
N
North China
South China
Yangtze Block
Cathaysia Block
Uplift
Chengdu
Chongqing
Guiyang
Kunming
Nanning
Guangzhou
Changsha
Wuhan
Hefei
Nanjing
Shanghai
Hangzhou
Fuzhou
Platform
Transitional zone
Slope/Basin
Investigated section
Previously studied sections

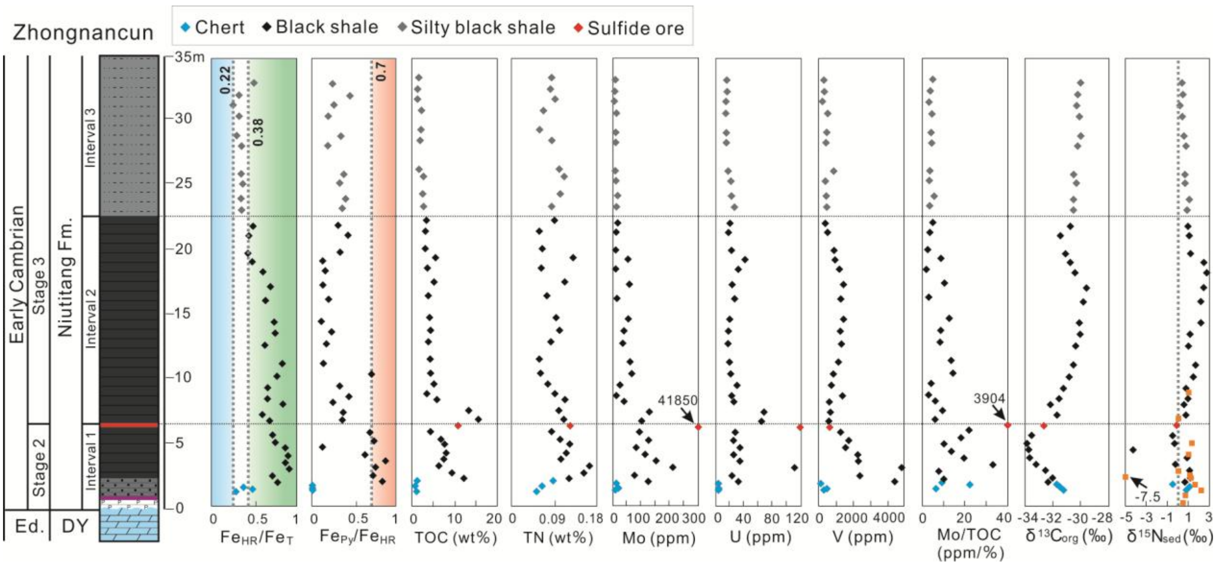
Zhongnancun
Chert
Black shale
Silty black shale
Sulfide ore
Early Cambrian
Stage 3
Stage 2
Niutitang Fm.
Interval 3
Interval 2
Interval 1
Ed.
DY
35m
30
25
20
15
10
5
0
0.22
0.38
0.7
41850
3904
-7.5
Fe_HR/Fe_T
Fe_Py/Fe_HR
TOC (wt%)
TN (wt%)
Mo (ppm)
U (ppm)
V (ppm)
Mo/TOC (ppm/%)
δ13Corg (‰)
δ15Nsed (‰)

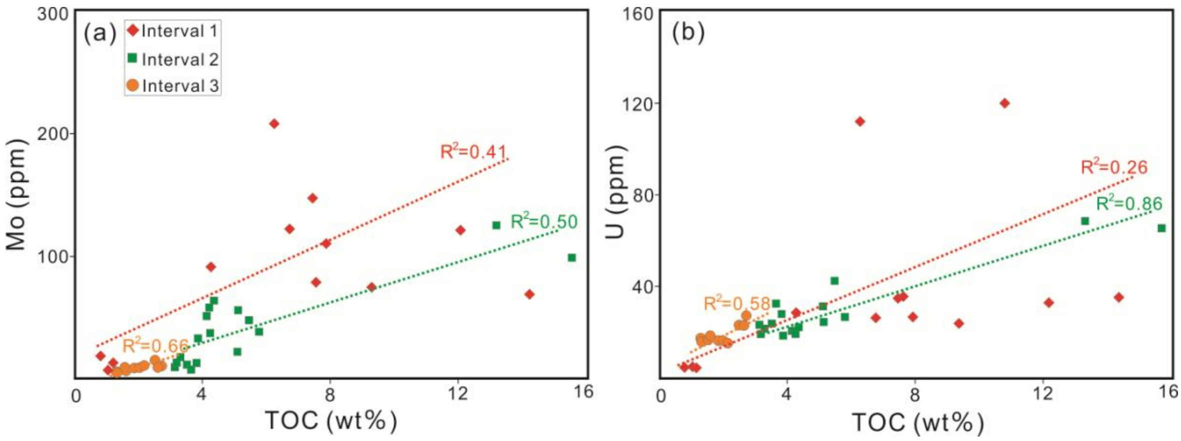
(a)
Interval 1
Interval 2
Interval 3
Mo (ppm)
TOC (wt%)
R^2=0.41
R^2=0.50
R^2=0.66
(b)
U (ppm)
TOC (wt%)
R^2=0.26
R^2=0.86
R^2=0.58

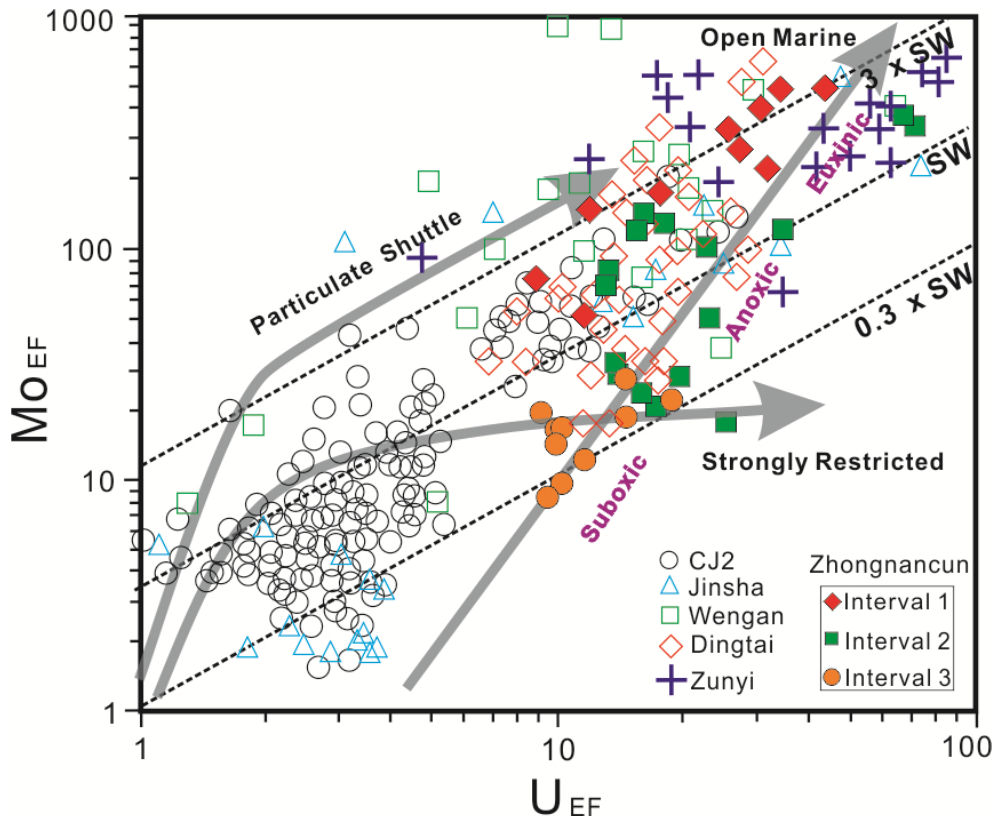

1000
100
10
1
1
10
100
Mo EF
U EF
Open Marine
3 x SW
SW
0.3 x SW
Particulate Shuttle
Euxinic
Anoxic
Suboxic
Strongly Restricted
CJ2
Jinsha
Wengan
Dingtai
Zunyi
Zhongnancun
Interval 1
Interval 2
Interval 3

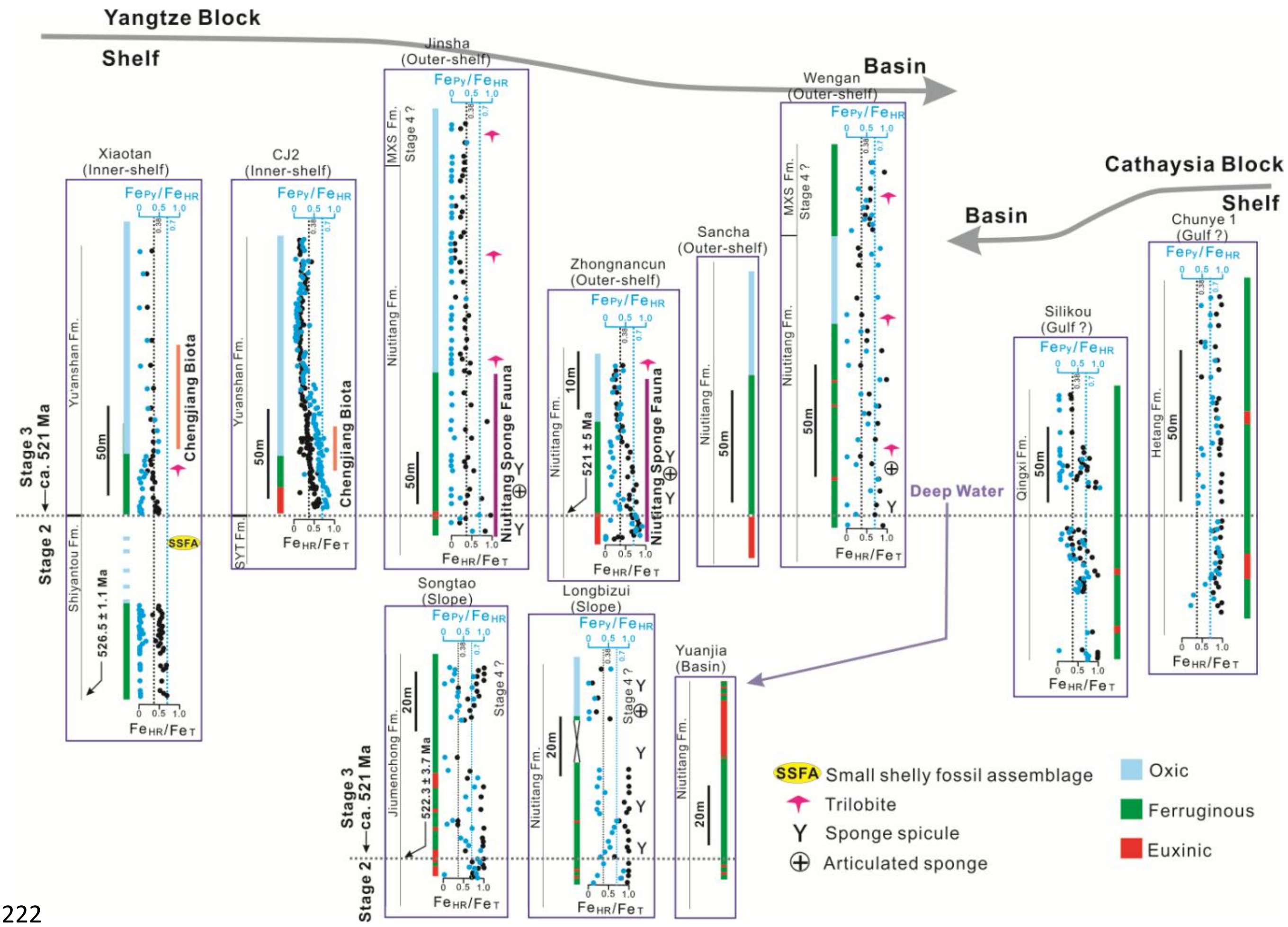

Yangtze Block
Shelf
Basin
Cathaysia Block
Shelf
Basin
Deep Water
Xiaotan (Inner-shelf)
CJ2 (Inner-shelf)
Jinsha (Outer-shelf)
Zhongnancun (Outer-shelf)
Sancha (Outer-shelf)
Wengan (Outer-shelf)
Silikou (Gulf ?)
Chunye 1 (Gulf ?)
Songtao (Slope)
Longbizui (Slope)
Yuanjia (Basin)
Stage 3 ← ca. 521 Ma
Stage 2
Chengjiang Biota
Niutitang Sponge Fauna
526.5 ± 1.1 Ma
521 ± 5 Ma
522.3 ± 3.7 Ma
Yu'anshan Fm.
Shiyantou Fm.
SYT Fm.
MXS Fm.
Niutitang Fm.
Qingxi Fm.
Hetang Fm.
Jiumenchong Fm.
Stage 4 ?
FePy/FeHR
FeHR/FeT
SSFA Small shelly fossil assemblage
Trilobite
Sponge spicule
Articulated sponge
Oxic
Ferruginous
Euxinic

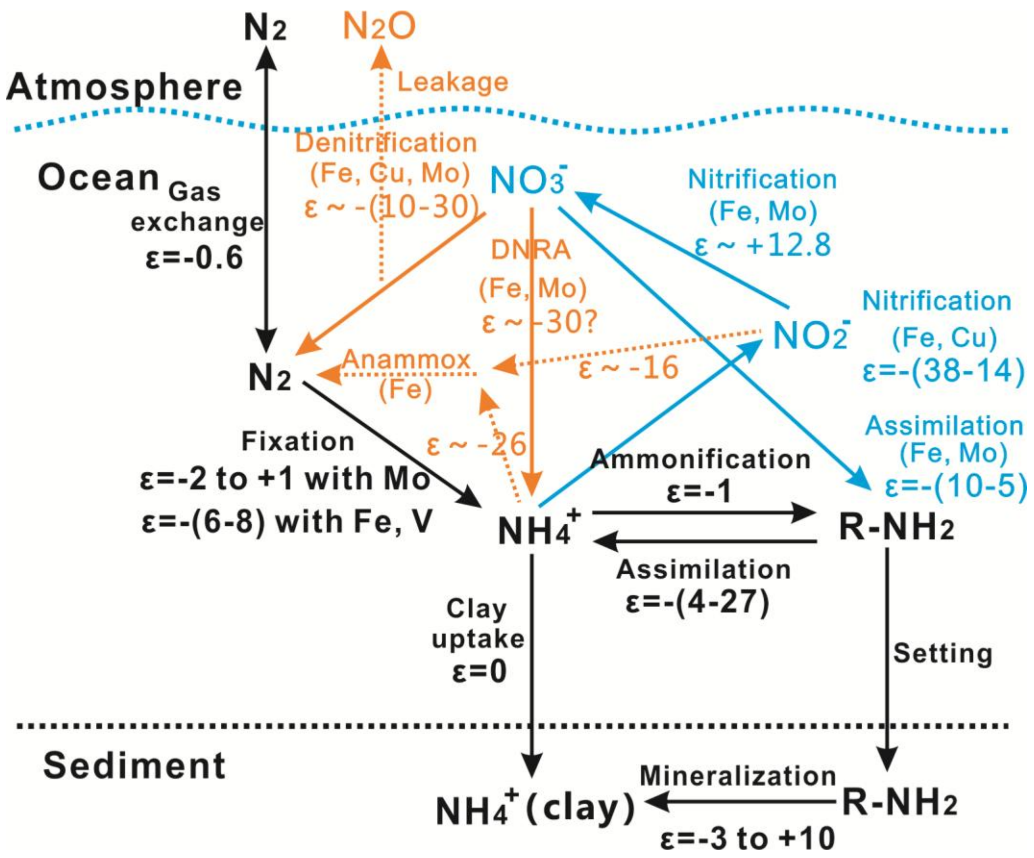

N2
N2O
Leakage
Atmosphere
Ocean
Gas exchange
ε=-0.6
Denitrification
(Fe, Cu, Mo)
ε ~ -(10-30)
NO3-
Nitrification
(Fe, Mo)
ε ~ +12.8
DNRA
(Fe, Mo)
ε ~ -30?
Nitrification
(Fe, Cu)
ε=-(38-14)
NO2-
ε ~ -16
N2
Anammox
(Fe)
ε ~ -26
Fixation
ε=-2 to +1 with Mo
ε=-(6-8) with Fe, V
Assimilation
(Fe, Mo)
ε=-(10-5)
Ammonification
ε=-1
NH4+
R-NH2
Assimilation
ε=-(4-27)
Clay
uptake
ε=0
Setting
Sediment
Mineralization
NH4+(clay)
R-NH2
ε=-3 to +10

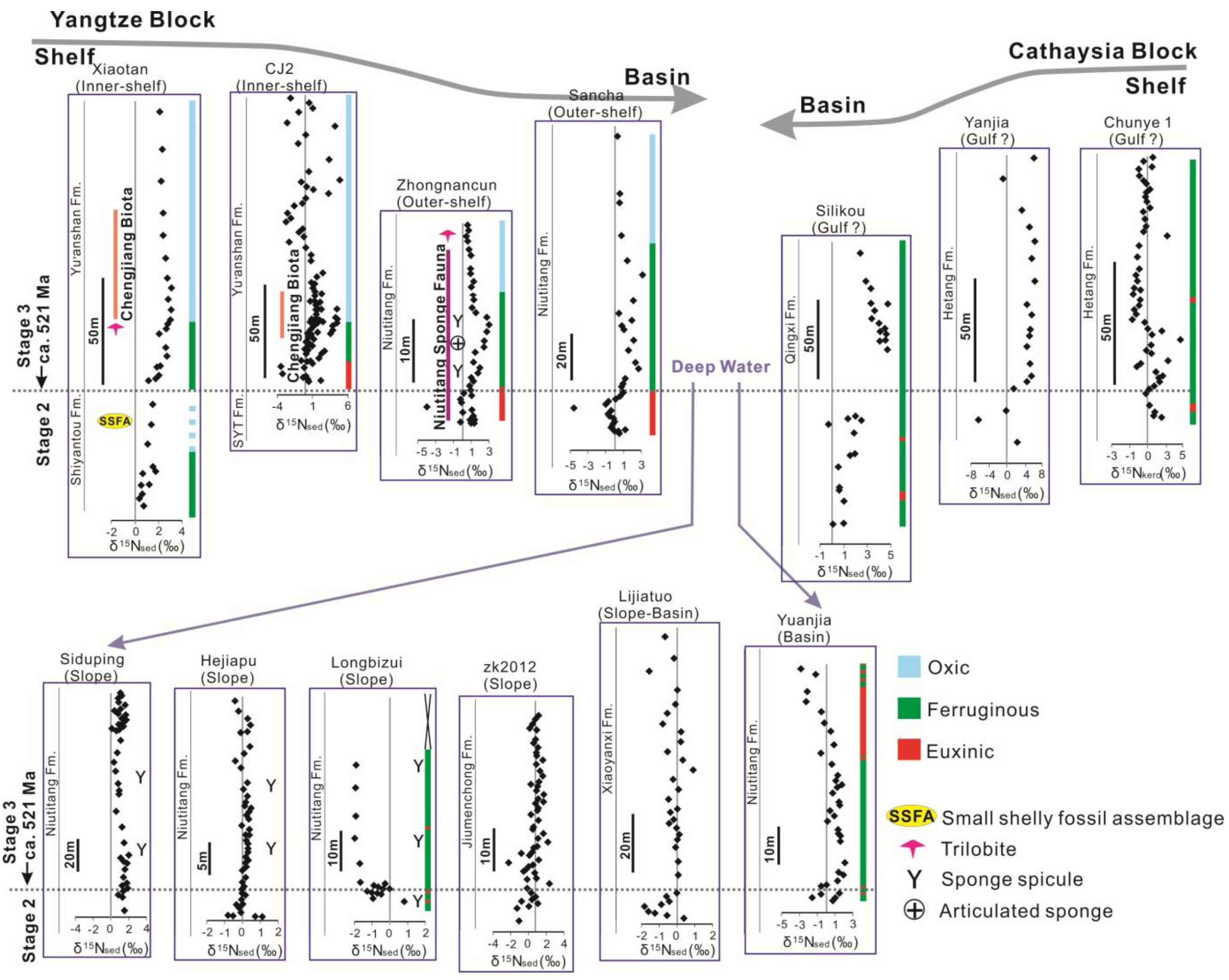

Yangtze Block
Shelf
Basin
Cathaysia Block
Shelf
Basin
Deep Water
Xiaotan (Inner-shelf)
CJ2 (Inner-shelf)
Zhongnancun (Outer-shelf)
Sancha (Outer-shelf)
Silikou (Gulf ?)
Yanjia (Gulf ?)
Chunye 1 (Gulf ?)
Siduping (Slope)
Hejiapu (Slope)
Longbizui (Slope)
zk2012 (Slope)
Lijiatuo (Slope-Basin)
Yuanjia (Basin)
Stage 3 ca. 521 Ma
Stage 2
Yu'anshan Fm.
Shiyantou Fm.
SYT Fm.
Niutitang Fm.
Qingxi Fm.
Hetang Fm.
Jiumenchong Fm.
Xiaoyanxi Fm.
Chengjiang Biota
Niutitang Sponge Fauna
SSFA
50m
20m
10m
5m
δ15Nsed (‰)
δ15Nkero (‰)
Oxic
Ferruginous
Euxinic
SSFA Small shelly fossil assemblage
Trilobite
Sponge spicule
Articulated sponge

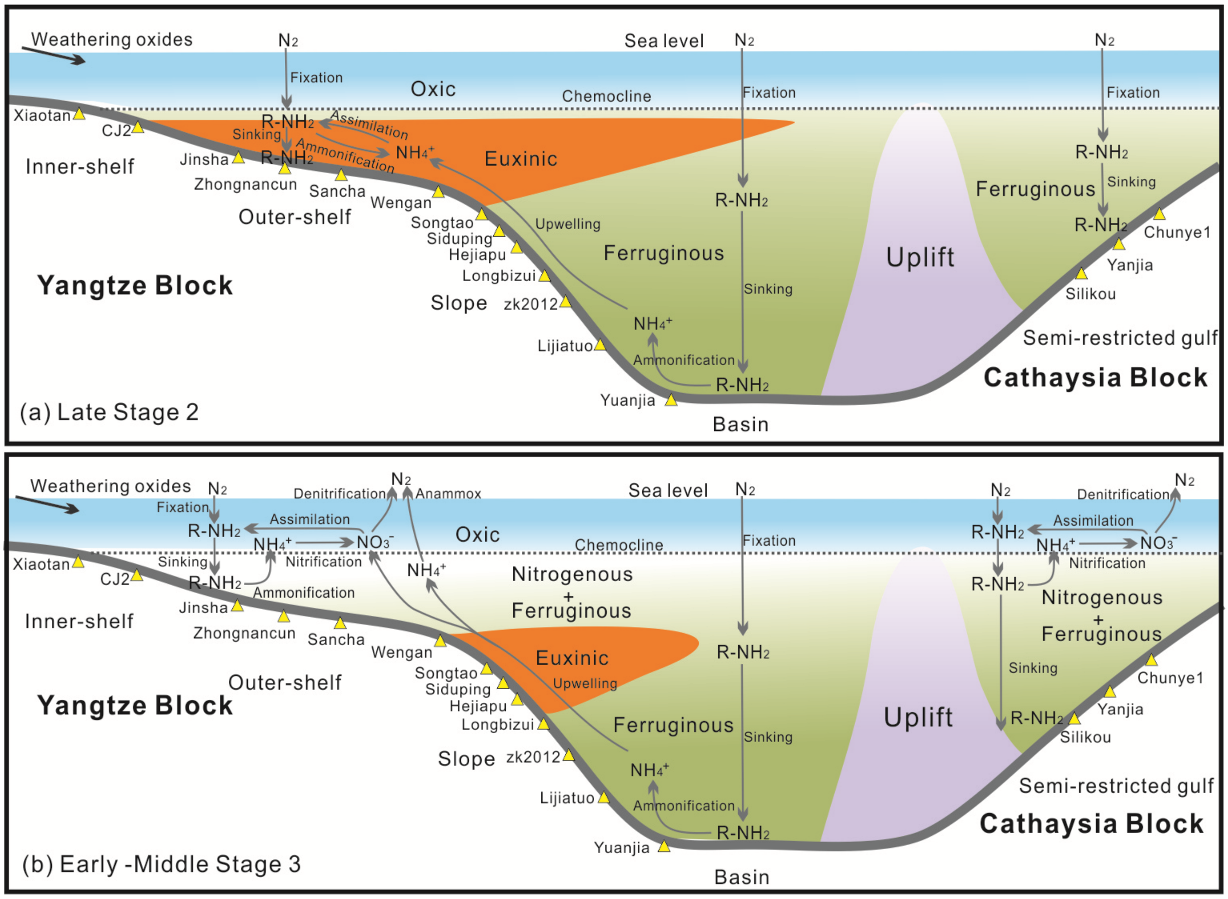
Weathering oxides
N2
Fixation
R-NH2
Sinking
R-NH2
Assimilation
Ammonification
NH4+
Oxic
Sea level
Chemocline
Euxinic
Xiaotan
CJ2
Jinsha
Zhongnancun
Sancha
Wengan
Inner-shelf
Outer-shelf
Songtao
Siduping
Hejiapu
Longbizui
Slope
zk2012
Lijiatuo
Yuanjia
Upwelling
Ferruginous
NH4+
Ammonification
R-NH2
N2
Fixation
R-NH2
Sinking
Basin
Uplift
N2
Fixation
R-NH2
Sinking
R-NH2
Ferruginous
Chunye1
Yanjia
Silikou
Semi-restricted gulf
Yangtze Block
Cathaysia Block
(a) Late Stage 2
Weathering oxides
N2
Fixation
R-NH2
Assimilation
NH4+
Nitrification
NO3-
Denitrification
N2
Anammox
Sinking
R-NH2
Ammonification
Oxic
Sea level
Chemocline
NH4+
Nitrogenous
+
Ferruginous
Euxinic
Upwelling
Ferruginous
NH4+
Ammonification
R-NH2
N2
Fixation
R-NH2
Sinking
Xiaotan
CJ2
Jinsha
Zhongnancun
Sancha
Wengan
Inner-shelf
Outer-shelf
Songtao
Siduping
Hejiapu
Longbizui
Slope
zk2012
Lijiatuo
Yuanjia
Basin
Uplift
N2
R-NH2
Assimilation
NH4+
NO3-
Nitrification
Denitrification
N2
R-NH2
Nitrogenous
+
Ferruginous
Sinking
R-NH2
Chunye1
Yanjia
Silikou
Semi-restricted gulf
Yangtze Block
Cathaysia Block
(b) Early -Middle Stage 3

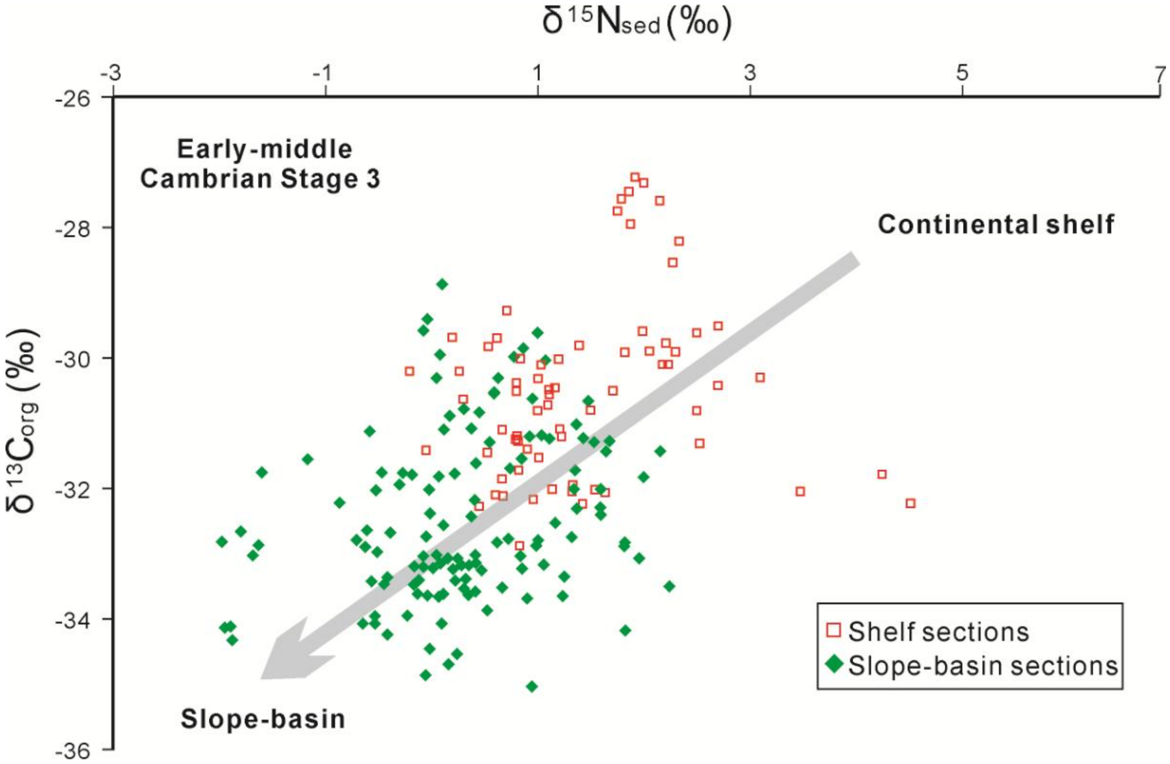
δ15Nsed (‰)
δ13Corg (‰)
Early-middle
Cambrian Stage 3
Continental shelf
Slope-basin
Shelf sections
Slope-basin sections
-3
-1
1
3
5
7
-26
-28
-30
-32
-34
-36

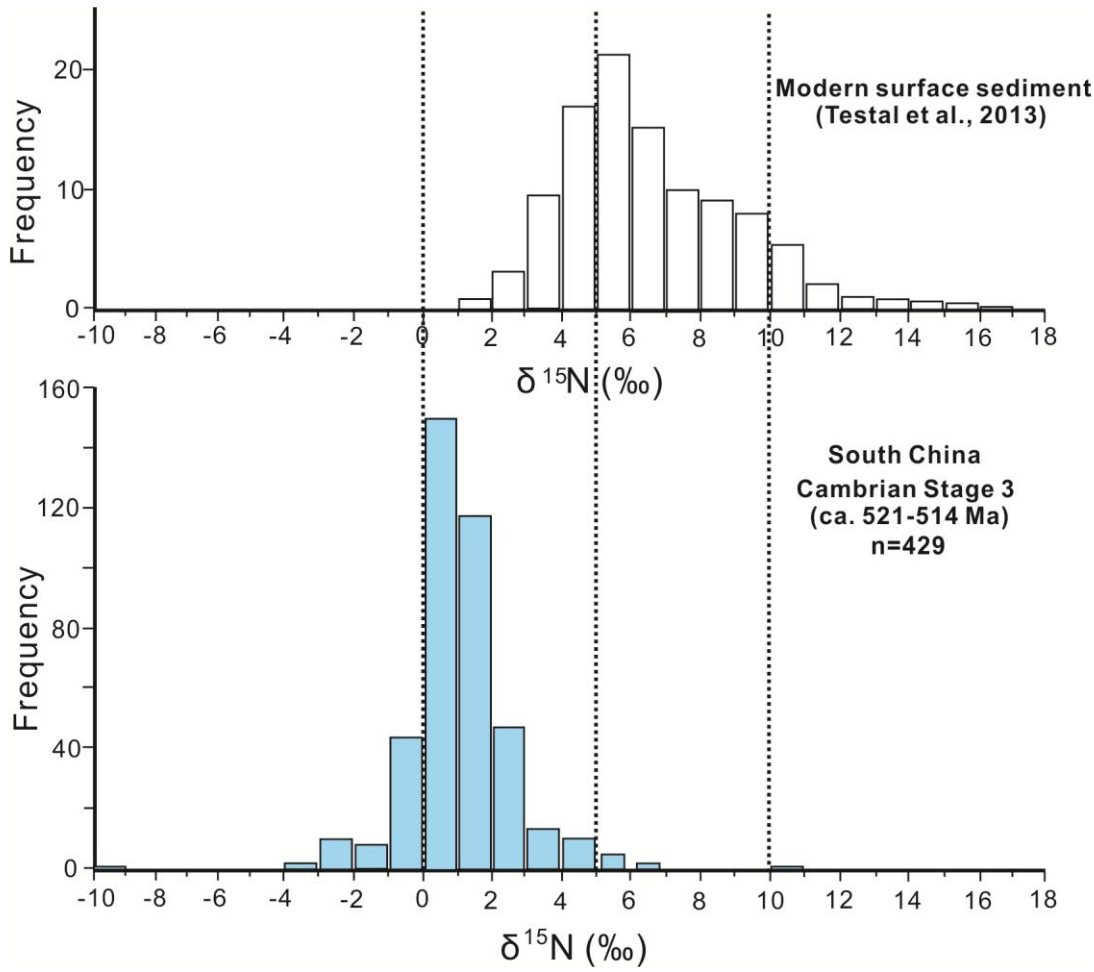
Frequency
Modern surface sediment
(Testal et al., 2013)
δ 15N (‰)
South China
Cambrian Stage 3
(ca. 521-514 Ma)
n=429
Frequency
δ 15N (‰)

Table S1
Click here to download Table: Supplementary Table S1.xlsx

Geochemical data for studied samples from Niutitang Formation at Zhongnancun section, South China.

Interval	Sample	Depth	Lithology	TOC (wt %)	Al (wt %)	Fe_T (wt %)	Fe_{HR}/Fe_T	Fe_{Py}/Fe_{HR}
3	ZNC40	33.4	Silty Black shale	1.56	10.38	1.60	0.48	0.17
3	ZNC39	32.5	Silty Black shale	1.32	10.47	1.85	0.26	0.42
3	ZNC38	31.7	Silty Black shale	1.35	10.26	1.98	0.21	0.19
3	ZNC37	30.8	Silty Black shale	2.18	10.15	2.15	0.26	0.11
3	ZNC36	29.3	Silty Black shale	2.04	10.08	1.85	0.23	0.29
3	ZNC35	28.5	Silty Black shale	1.87	9.80	1.25	0.30	0.11
3	ZNC34	26.3	Silty Black shale	1.62	9.72	1.68	0.29	0.33
3	ZNC33	25.6	Silty Black shale	2.65	9.54	1.32	0.31	0.27
3	ZNC32	24.3	Silty Black shale	2.52	10.03	1.47	0.29	0.36
3	ZNC31	23.5	Silty Black shale	2.73	8.82	2.46	0.29	0.31
2	ZNC30	22.2	Black shale	3.30	9.58	1.05	0.46	0.25
2	ZNC29	21.5	Black shale	3.18	8.32	1.34	0.40	0.39
2	ZNC28	20.1	Black shale	3.14	8.15	1.72	0.38	0.27
2	ZNC27	19.4	Black shale	5.46	7.42	0.92	0.45	0.02
2	ZNC26	18.6	Black shale	3.65	7.84	1.63	0.60	0.06
2	ZNC25	17.5	Black shale	5.12	8.23	1.03	0.71	0.03
2	ZNC24	16.4	Black shale	3.82	8.65	2.32	0.64	0.11
2	ZNC23	14.7	Black shale	4.13	8.20	1.15	0.77	0.01
2	ZNC22	13.8	Black shale	4.25	8.87	1.08	0.78	0.15
2	ZNC21	12.9	Black shale	3.87	8.68	1.21	0.63	0.08
2	ZNC20	11.4	Black shale	4.20	7.88	0.93	0.88	0.04
2	ZNC19	10.5	Black shale	4.36	8.46	0.86	0.80	0.72
2	ZNC18	9.6	Black shale	5.10	8.24	1.15	0.67	0.27
2	ZNC17	8.8	Black shale	3.52	9.13	1.23	0.67	0.40
2	ZNC16	8.3	Black shale	5.78	7.15	0.78	0.88	0.17
2	ZNC15	7.5	Black shale	13.20	6.20	1.21	0.60	0.32
2	ZNC14	6.8	Black shale	15.56	5.54	1.62	0.70	0.31
1	ZNC13	6.3	Sulfide ore	10.72	2.05	11.50	n.m.	n.m.
1	ZNC12	5.9	Black shale	4.27	9.87	2.56	0.67	0.78
1	ZNC11	5.3	Black shale	6.73	4.73	1.78	0.68	0.69
1	ZNC10	4.8	Black shale	7.56	6.75	2.13	0.87	0.74
1	ZNC09	4.2	Black shale	7.88	6.36	1.76	0.88	0.66
1	ZNC08	3.7	Black shale	7.45	6.87	2.52	0.84	0.85
1	ZNC07	3.2	Black shale	6.25	6.10	3.34	0.89	0.78
1	ZNC06	2.6	Black shale	9.30	5.32	2.78	0.72	0.71
1	ZNC05	2.3	Black shale	12.08	4.60	3.10	0.79	0.83
1	ZNC04	2.1	Chert	1.21	2.83	0.68	0.34	0.04
1	ZNC02	1.9	Chert	0.82	2.36	0.69	0.41	0.04
1	ZNC01	1.7	Chert	1.05	2.52	0.76	0.28	0.05

Table S2

Click here to download Table: Supplementary Table S2.xlsx

Fe speciation data for early Cambrian successions in the Yang

Sample	Formation	Height (m)	Fe_{HR}/Fe_T	Fe_{Py}/Fe_{HR}
Xiaotan section, Yunan, South China				
XTY61	Yu'anshan	380	0.33	0.02
XTY60	Yu'anshan	370	0.22	0.11
XTY59	Yu'anshan	355	0.22	0.01
XTY58	Yu'anshan	340	0.34	0.22
XTY57	Yu'anshan	329	0.3	0.02
XTY56	Yu'anshan	319	0.39	0.22
XTY55	Yu'anshan	310	0.3	0.24
XTY54	Yu'anshan	305	0.3	0.42
XTY53	Yu'anshan	300	0.39	0.46
XTY52	Yu'anshan	295	0.35	0.5
XTY51	Yu'anshan	290.5	0.37	0.47
XTY50	Yu'anshan	288.5	0.35	0.18
XTY49	Yu'anshan	286.7	0.28	0.15
XTY48	Yu'anshan	284.7	0.3	0.16
XTY47	Yu'anshan	281.7	0.23	0.08
XTY46	Yu'anshan	280.8	0.35	0.16
XTY45	Yu'anshan	279.3	0.35	0.13
XTY44	Yu'anshan	278.3	0.34	0.02
XTY43	Yu'anshan	277	0.41	0.06
XTY42	Yu'anshan	274	0.33	0.08
XTY41	Yu'anshan	270	0.35	0.09
XTY40	Yu'anshan	268.3	0.46	0.05
XTY39	Yu'anshan	266.3	0.4	0
XTY38	Yu'anshan	265.3	0.47	0.01
XTY37	Yu'anshan	264.6	0.49	0.05
XTY36	Yu'anshan	264	0.41	0.01
XTY35	Yu'anshan	263	0.51	0.08
XTY30	Shiyantou	222	0.51	0
XTY29	Shiyantou	220.6	0.5	0
XTY28	Shiyantou	219.6	0.55	0.04
XTY27	Shiyantou	218.6	0.59	0
XTY26	Shiyantou	217.6	0.36	0.09
XTY25	Shiyantou	216.6	0.58	0.01
XTY24	Shiyantou	215.6	0.55	0.01
XTY23	Shiyantou	214.6	0.53	0.04
XTY22	Shiyantou	213.6	0.52	0.01
XTY21	Shiyantou	212.6	0.59	0
XTY20	Shiyantou	211.64	0.58	0.07
XTY19f	Shiyantou	211.44	0.58	0.01
XTY19e	Shiyantou	211.27	0.54	0.01

Table S3
Click here to download Table: Supplementary Table S3.xlsx

$\delta^{15}N_{sed}$ and $\delta^{13}C_{org}$ data for early Cambrian successions in the Yangtze Block.

Sample	Formation	Height (m)	$\delta^{15}N_{sed}$ (‰)	$\delta^{13}C_{org}$ (‰)	Data Sources
Xiaotan section, Yunan, South China					
XTY 61	Yu'anshan	611.6	2.4	-25.1	Cremonese et al., 2013
XTY 60	Yu'anshan	591.6	2.7	-31.9	Cremonese et al., 2013
XTY 59	Yu'anshan	576.6	2.5	-27.8	Cremonese et al., 2013
XTY 58	Yu'anshan	561.6	2.7	-27.0	Cremonese et al., 2013
XTY 57	Yu'anshan	550.6	2.7	-27.9	Cremonese et al., 2013
XTY 56	Yu'anshan	540.6	2.6	-26.4	Cremonese et al., 2013
XTY 55	Yu'anshan	531.6	2.7	-26.8	Cremonese et al., 2013
XTY 54	Yu'anshan	526.6	2.7	-27.3	Cremonese et al., 2013
XTY 53	Yu'anshan	521.6	2.5	-26.0	Cremonese et al., 2013
XTY 52	Yu'anshan	516.6	2.8	-28.9	Cremonese et al., 2013
XTY 51	Yu'anshan	511.6	2.8	-29.1	Cremonese et al., 2013
XTY 50	Yu'anshan	509.6	2.5	-26.2	Cremonese et al., 2013
XTY 49	Yu'anshan	507.8	2.7	-27.6	Cremonese et al., 2013
XTY 48	Yu'anshan	505.8	1.8	-28.6	Cremonese et al., 2013
XTY 44	Yu'anshan	499.4	2.2	-28.4	Cremonese et al., 2013
XTY 43	Yu'anshan	498.1	2.3	-28.5	Cremonese et al., 2013
XTY 42	Yu'anshan	495.1	2.3	-28.2	Cremonese et al., 2013
XTY 41	Yu'anshan	491.1	2.2	-27.6	Cremonese et al., 2013
XTY 40	Yu'anshan	489.5	1.9	-28.0	Cremonese et al., 2013
XTY 39	Yu'anshan	487.5	1.9	-27.2	Cremonese et al., 2013
XTY 38	Yu'anshan	486.5	2.0	-27.3	Cremonese et al., 2013
XTY 37	Yu'anshan	485.8	1.9	-27.4	Cremonese et al., 2013
XTY 36	Yu'anshan	485.2	1.8	-27.8	Cremonese et al., 2013
XTY 35	Yu'anshan	484.2	1.8	-27.6	Cremonese et al., 2013
XTY 34	Shiyantou	483.2	1.2	-28.8	Cremonese et al., 2013
XTY 33	Shiyantou	473.2	1.5	-29.5	Cremonese et al., 2013
XTY 32	Shiyantou	463.2	1.4	-30.4	Cremonese et al., 2013
XTY 31	Shiyantou	453.2	1.1	-30.5	Cremonese et al., 2013
XTY 30	Shiyantou	443.2	1.5	-29.7	Cremonese et al., 2013
XTY 29	Shiyantou	441.7	1.7	-30.0	Cremonese et al., 2013
XTY 28	Shiyantou	440.7	0.6	-29.9	Cremonese et al., 2013
XTY 27	Shiyantou	439.7	0.9	-30.4	Cremonese et al., 2013
XTY 26	Shiyantou	438.7	0.9	-29.8	Cremonese et al., 2013
XTY 25	Shiyantou	437.7	0.6	-29.4	Cremonese et al., 2013
XTY 24	Shiyantou	436.7	1.0	-29.6	Cremonese et al., 2013
CJ2 section, Yunan, South China					
	Yu'anshan	55.8	-2.2	-29.7	Hammarlund et al., 2017
	Yu'anshan	59.0	0.6	-29.5	Hammarlund et al., 2017
	Yu'anshan	61.8	1.0	-29.8	Hammarlund et al., 2017
	Yu'anshan	64.0	-0.9	-29.8	Hammarlund et al., 2017